SEISMIC EXPRESSION, STRUCTURE, AND EVOLUTION OF FLOW CELLS WITHIN A SUBMARINE LANDSLIDE

HARYA D. NUGRAHA[1*], CHRISTOPHER A-L. JACKSON[2,3], HOWARD D. JOHNSON[2], and DAVID M. HODGSON[4]

[1]*Center for Sustainable Geoscience and Outreach, Universitas Pertamina, Jakarta 12220, Indonesia*
[2]*Landscapes and Basins Research Group (LBRG), Imperial College, London SW7 2BP, UK*
[3]*WSP, Manchester M15 4RP, UK*
[4]*Stratigraphy Group, School of Earth and Environment, University of Leeds, Leeds LS2 9JT, UK*

**email: harya.dn@universitaspertamina.ac.id*

Keywords: submarine landslide, mass-transport complex, seismic reflection, intra-flow shear, flow cells

ABSTRACT

Submarine landslides (slides) are not a singular mass of sediment, but may instead comprise shear zone-bound, intra-flow cells of different sizes, rheological states, and strains. Constraining the sizes and evolution of these cells is important for assessing the risk slides pose to subaqueous infrastructure and coastal communities. However, controls on their initiation, translation, and cessation remain unclear. We here use five, high-quality post-stack time-migrated (PSTM) 3D seismic reflection datasets to define the seismic expression and investigate the structure and evolution of cells in the Gorgon Slide, a near-seabed submarine landslide on the Exmouth Plateau, offshore NW Australia. Our data suggest that the slide originated from a 30 km-wide, NE-trending headwall scarp that dips steeply (c.30^{o}) seaward, and travelled northwestwards over a strongly erosional basal-shear surface that deepens downdip. The slide is dominated by chaotic seismic reflections, interpreted as debrite, containing large clasts (up to 1 km-long) derived from the headwall. The morphology and orientation of the basal-shear surface focused slide transport, resulting in clustering of megaclasts in the medial part of the still-translating flow. This cluster became an obstacle to flow, resulting in two flow cells (Cells A and B), separated by a longitudinal shear zone. Interaction between the cells is recorded by sinuous flow fabrics within, and pressure ridges on the top surface of, the slide. The intra-flow fabrics and top-surface ridges in Cell A were dragged downdip by the relatively faster moving and/or longer-lasting Cell B, which continued translating downdip without intra-flow obstacles. The transport and emplacement processes inferred for the Gorgon Slide suggest that entrainment and abrasion of megaclasts can induce velocity perturbations during slide emplacement, causing changes in flow rheology, and the initiation and cessation of flow cells. Understanding how flow cells evolve may help refine attempts to model their potential damaging impact on subaqueous infrastructure.

INTRODUCTION

Subaqueous landsliding can trigger the emplacement of slides, which typically comprise clast-bearing debrite (e.g. Dott, R., 1963; Nardin, T. R. *et al.*, 1979; Nemec, W., 1991; Moscardelli, L. & Wood, L., 2008; Posamentier, H. W. & Martinsen, O. J., 2011). Subaqueous landslides can evolve temporally and spatially. For example, a relatively large slide (i.e., first-order flow cell; *sensu* Alsop and Marco, 2014) may entrain ambient water, causing it to become more dilute and increasing in intra-flow turbulence, (Fisher, R. V., 1983; Talling, P. J. *et al.*, 2012; Sun, Q. *et al.*, 2018a). Field studies of metre-scale slides (referred to as 'slumps' by Alsop, G. I. & Marco, S., 2014) show that these first-order cells can also break-down into second-order (i.e., intra-flow) cells, between which strain styles, patterns, and magnitudes can abruptly vary (Farrell, S. G., 1984; Alsop, G. I. & Marco, S., 2014). Alsop, G. I. and Marco, S. (2014) propose that these complexities arise due to local (i.e., intra-flow) variations in: (i) the lithology and stratigraphic architecture of the failed and translating sediment mass; (ii) fluid pressure within and below the translating sediment mass; and (iii) the attitude of the basal-shear surface, or *décollement*, underlying the translating sediment mass. Although these studies are undoubtedly informative, it is unclear if the structures observed within, and models developed from, these relatively small-scale 2D exposures are applicable at much larger scales.

A few 3D seismic reflection data-based studies have documented cells that are significantly larger (i.e., decametre-scale) than those identified in the field. These cells occur within relatively long run-out deposits emplaced by one (Gee, M. *et al.*, 2005; Steventon, M. J. *et al.*, 2019; Abu, C. *et al.*, 2022) or more (Gee, M. *et al.*, 2005; Bull, S. *et al.*, 2009) flows. For example, using 3D seismic reflection data from offshore Uruguay, Steventon, M. J. *et al.* (2019) show that up to 18 km-wide cells developed in the contractional domain of a large, megaclast-bearing slide. Cells are defined by differing magnitudes of contractional strain (i.e., thrusts and related folds), and they are bound by up to 35 km-long shear zones. The mechanism for cell development in this case is unclear, although they seem to record some combination of an abrupt or progressive lateral variation in flow velocity, and/or the total amount of

emplacement-related strain (see also Bull, S. *et al.*, 2009). Thus, despite a growing body of work on the structure and kinematics of intra-flow cells, the mechanisms responsible for their initiation, translation, and cessation, across a range of scales, remain poorly understood. Progress towards mitigating the geohazards associated with subaqueous landsliding at least partly depends on a thorough understanding of their emplacement processes, including cell formation (Masson, D. *et al.*, 2006). For example, the rheology and emplacement direction of a slide can change during transport (Iverson, R. M., 1997; Dykstra, M. *et al.*, 2011; Joanne, C. *et al.*, 2013; Ortiz-Karpf, A. *et al.*, 2017; Hodgson, D. *et al.*, 2018), which may influence the amount and direction of drag forces exerted on subaqueous pipelines (e.g., Zakeri, A., 2009).

Here, we use five high-quality 3D seismic reflection datasets from the Exmouth Plateau (offshore NW Australia) to study the Gorgon Slide (Fig. 1). The slide is at or just below the seabed and is accordingly well-imaged, meaning we can: (i) use a range of seismic attributes to map kinematic indicators below, within, and above the slide; (ii) define and map intra-slide cells; (iii) reconstruct slide emplacement, inferring the impact cell formation and evolution had on overall flow behaviour; and (iv) consider the potential factors controlling cell formation. We therefore test existing models for cell formation within sediment gravity-flows and assess the implications of our work for understanding their related geohazard.

DATA AND METHODOLOGY

The five, high-quality post-stack time-migrated (PSTM) 3D seismic reflection datasets image *c.*93% (i.e. 1594 km^2 of 1760 km^2 total area) of the Gorgon Slide, covering all of the evacuation zone and most of the deposition zone (Figs. 1B-C). We used three 2D seismic reflection lines to constrain the downdip limit of the deposition zone (green lines in Fig. 1C). The vertical resolution of the 3D seismic reflection data at the base of the slide (*c.*500 m below sea floor) ranges from 8-11 m, based on near seabed sediment velocity and dominant seismic frequency of 1824 m/s and 40-60 Hz, respectively. Bin spacing

of the 3D seismic volumes ranges from 12.5 x 18.75 m to 20 x 25 m (see Appendix 1 for details). Depth conversion of seabed and basal-shear surface time-structure maps was conducted by using average seismic velocities for water (1519 m/s) and weakly compacted, near-seabed sediment (1824 m/s), respectively (Appendix 1). The average water velocity is constrained by ten industry wells (Fig. 1B), and the near-seabed sediment velocity data is available from well ODP 762 (see Figs. 1A and 2).

We mapped the seabed and basal-shear surface of the Gorgon Slide to define its kinematics as it initiated, translated, and arrested. We also employed an iso-proportional slicing method (Zeng, H. *et al.*, 1998), midway between the seabed and basal-shear surface of the slide, to visualise and map the heterogeneity of its constituent seismic facies. Several seismic attributes were used in this analysis, particularly: (i) *variance*, to better image discontinuities (Chopra, S. & Marfurt, K. J., 2007), including grooves on the basal-shear surface of a slide (e.g., Bull, S. *et al.*, 2009); (ii) *Root Mean Squared (RMS) Amplitude*, to better delineate features that have distinct positive or negative amplitudes resulting from an acoustic (velocity and/or density) contrast (Brown, A. R., 2011), such as megaclasts encased within a relatively transparent debritic matrix (e.g., Ortiz-Karpf, A. *et al.*, 2017); (iii) *dip*, to better image rugosity of a surface (Brown, A. R., 2011), including seabed relief (e.g., Bull, S. *et al.*, 2009); and (iv) *spectral decomposition*, to highlight internal stratigraphic (seismic facies) heterogeneities within a geological body such as a slide (Partyka, G. *et al.*, 1999; Eckersley, A. J. *et al.*, 2018).

GEOLOGICAL SETTING

The Exmouth Plateau is a part of North Carnarvon Basin, which has experienced multiple rifting events from the Late Jurassic to Early Cretaceous (Fig. 2) (Tindale, K. *et al.*, 1998; Longley, I. M. *et al.*, 2002). Post-rift deposition was initially dominated by fine-grained siliciclastic sediments, becoming carbonate-dominated as the Australian plate drifted northward towards the equator (e.g., Apthorpe, M., 1988; Hull, J. N. F. & Griffiths, C. M., 2002). Seismically imaged clinoforms and borehole data demonstrate progradation of the carbonate-dominated margin from the Oligocene to the present-day

(Fig. 2B) (Cathro, D. L. *et al.*, 2003; Moss, G. D. *et al.*, 2004). Collision between the Australian and Eurasian plates (Miocene to present-day) has reactivated some of the rift-related faults, forming inversion structures such as the NE-trending Exmouth Plateau Arch (Fig. 2) (Keep, M. *et al.*, 1998). It is likely that inversion-related deformation of the seabed triggered the widespread emplacement of the numerous carbonate-dominated, sediment gravity-driven deposits across the plateau, including the focus of this study, the Gorgon Slide, which extends from the seabed (blue) down to its basal-shear surface (yellow, see Fig. 2B) (Boyd, R. *et al.*, 1993; Hengesh, J. V. *et al.*, 2013; Scarselli, N. *et al.*, 2013; Wu, N. *et al.*, 2026). The headwall of the Gorgon Slide is underlain by a rift-related horst block, which was drilled by Bluebell-1 (Fig. 2B) (McCormack, K. & McClay, K., 2013).

THE GORGON SLIDE

General Characteristics

External geometry and morphological domains.– The Gorgon Slide was sourced from the slope defining the present-day shelf-edge of NW Australia (Fig. 1). It was deposited in the adjacent Kangaroo Syncline, forming a lenticular, NW-trending body that wedges-out (i) to the SE against the continental slope, and (ii) to the NW against the eastern margin of the Exmouth Plateau Arch (see Figs. 1B-C and 2). The slide has a maximum runout distance of *c.*70 km, is up to 500 m-thick, and has a total volume of *c.*500 km^3 (Fig. 3A) (Nugraha, H. D. *et al.*, 2022). The slide terminates against two lateral margins (to the NE and SW), being *c.*30 km-wide in the central part and abruptly narrowing to *c.*18 km at its frontal end (Fig. 3A). Downdip changes in the slide width results in two relatively steeply dipping (18°) frontal margins (eastern and western), separated by *c.*10 km in the dip-direction by a NW-trending lateral margin (Fig. 3A).

The central and frontal parts of the slide display a notable along-strike change in seabed rugosity, which defines two distinctive regions: Areas A and B (Fig 3B). Area A is bound by the NE lateral and eastern frontal margins and is characterized by a highly rugose seabed (Fig. 3B). In Area B, which is

bound by the SW lateral and western frontal margins, the seabed is relatively smoother than that of Area A (Fig. 3B). Areas A and B are separated by a linear, NW-trending feature (see zoomed-in image in Fig. 3B) that is subparallel to both lateral margins of the slide. This feature is narrow (*c.*170-300 m-wide) and extends for *c.*26 km updip, apparently dying-out where Areas A and B merge and become indistinguishable, and merging downdip with the NE lateral margin of Area B near the slide terminus (see Figs. 3B-C). This feature marks a change in seabed relief of *c.*10-20 m between Areas A and B (Fig. 3C). We interpret the linear feature on the seabed (Figs. 3B-C) as a longitudinal shear zone (sensu Bull, S. *et al.*, 2009), which records internal variations of transport velocity within the slide (see also Steventon, M. J. *et al.*, 2019). This longitudinal shear zone is interpreted at this point in the paper because it later helps us define and describe different structural domains within the slide.

The Gorgon Slide originated from a *c.*18 km-long evacuation zone, bound on its updip margin by a relatively steeply-dipping (*c.*30^{o}), *c.*350 m-high headwall scarp (Fig. 4A). We note that this scarp is relatively simple, being defined by a single, smooth, seaward-facing plane, rather than by a composite, staircase-like morphology. The frontal margin of Area A is clearly marked by positive seabed relief (*c.*30 m) relative to the smooth seabed bounding pre-slide slope strata immediately downdip. Pre-slide strata are represented by older gravity-driven (i.e., chaotic, weakly reflective seismic reflections), and hemipelagic and pelagic slope strata (i.e., continuous, reflective, sub-parallel seismic reflections) (Fig. 4A). The juxtaposition of seismically chaotic, interpreted debrite-rich, strata can make establishing stratigraphic relationships challenging, not least because the kinematic development of a slide basal-shear surface can also involve remobilization and deformation of older strata (e.g., Butler and McCaffrey, 2010; Hodgson et al., 2018). Nonetheless, we differentiate between the Gorgon Slide and pre-slide strata based on the observation that: (i) hemipelagic and pelagic slope strata being sharply truncated along the basal-shear surface of the Gorgon Slide (Fig. 4); (ii) older slide being capped by hemipelagic and pelagic slope strata (paleo-seabed), strongly suggesting periods of non-gravity-driven deposition between events associated with their emplacement (Fig. 4B); and (iii) a

relatively thin interval of the Gorgon Slide material caps and is thus demonstrably younger than the hemipelagic and pelagic slope strata capping older slide (Fig. 4B).

Internal seismic facies.– The Gorgon Slide contains a range of seismic facies that we infer record deposition by a range of sediment transport processes, and that reflect variable strain styles (Fig. 5) (e.g., Alves, T. M. *et al.*, 2014). Our seismic facies classification draws on studies that have calibrated seismic reflection data with lithology from well data (e.g., Sawyer, D. E. *et al.*, 2009), and which have used field data to construct seismic reflection forward models (Dykstra, M. *et al.*, 2011). We define five seismic facies (SF) (Fig. 5A) based on variations in reflection strength and internal deformation (see Figs. 5B-G): (i) SF-1 – low-to-variable amplitude, chaotic reflections - these are interpreted as debrites (cf. Posamentier, H. W. & Kolla, V., 2003; Posamentier, H. W. & Martinsen, O. J., 2011; Ortiz-Karpf, A. *et al.*, 2017); (ii) SF-2 – low-to-medium amplitude, discontinuous reflections that are folded in cross-section, and that are associated with very well-developed sinuous lineations within and at the top of the slide in plan-view – these are also interpreted as debrites containing seismic-scale clasts, and which contain pressure ridges (Bull, S. *et al.*, 2009); (iii) SF-3 – high-amplitude, relatively continuous, folded reflections that are offset by thrusts – these are interpreted as fold and thrust systems developed within relatively cohesive portions of the slide; (iv) SF-4 – packages of relatively continuous, sub-parallel, variably deformed reflections that are surrounded by SF-1 and -2 and that extend vertical through the entire thickness of the deposit – these are interpreted as megaclasts embedded within the debritic matrix (cf. McGilvery, T. A. H., Geoffrey, 2004; Bull, S. *et al.*, 2009; Jackson, C. A., 2011; Ortiz-Karpf, A. *et al.*, 2017; Hodgson, D. *et al.*, 2018); and (v) SF-5 – variable amplitude, continuous, sub-parallel reflections – these are interpreted as pelagic and hemipelagic slope strata (see Fig. 4A) (e.g., Prélat, A. *et al.*, 2015). The *c.*26 km-long, NW-trending longitudinal shear zone described above is generally characterised by SF-1 (Fig. 3C) (i.e. debrite) (cf. Ogata, K. *et al.*, 2014; Bull, S. & Cartwright, J. A., 2019; Omeru, T. & Cartwright, J. A., 2019), although its relatively narrow width means it can be difficult to differentiated it from adjacent deposits within Area A and B

where more continuous reflections (i.e. megaclasts; SF-4) are not juxtaposed across it (Figs. 4B, and 5B-E).

Having provided a general overview of the external geometry, scale, and inferred composition of the Gorgon Slide, and the processes involved in its deposition, we now provide a systematic description of its primary kinematic indicators and interpret the related emplacement processes from its four principal domains: (i) the headwall domain; (ii) the upper translational domain (UTD); (iii) the lower translational domain (LTD); and (iv) the toe domain (Fig. 3B).

Headwall domain

Description.– The largest feature in the headwall domain is a large, NW-dipping scarp (Fig. 6). Immediately updip of this feature are: (i) a small, NNE-trending scarp, next to which are (ii) numerous circular depressions that have diameters of *c.*100-300 m, and (iii) at least four, *c.*3-5 km-long, *c.*15 m-deep, linear depressions (see zoomed-in image in Fig. 6A). Downdip of the headwall scarp, within the source area of the Gorgon Slide (i.e. the region between the headwall scarp and evacuation-deposition zone boundary), there are numerous *c.*5-16 km-long, broadly NW-trending, elongate features (Figs. 6A-B) that have a v-shaped geometry in cross-section, which are (*c.*150-300 m-wide and *c.*10-25 m-deep (see zoomed-in image in Fig. 6B).

Interpretation.– The small scarp (*c.*10 m-high) is cross-cut by, and thus older than, the main headwall scarp (Fig. 6B). This smaller, older scarp may have been associated with a slope failure responsible for deposition of one or several of the older, thinner, pre-slide gravity-driven deposits underlying the Gorgon Slide (Fig. 4). The circular depressions are interpreted as pockmarks (e.g., Hengesh, J. V. *et al.*, 2013; Scarselli, N. *et al.*, 2013), which could indicate active vertical fluid expulsion. The linear depressions are interpreted as crown cracks, possibly marking the location of future slope failure events (Varnes, D. J., 1978; Frey-Martinez, J. *et al.*, 2005). We interpret the elongate features with v-shaped cross-sectional geometry as grooves (sensu Bull, S. *et al.*, 2009) formed due to tooling by

megaclasts into the substrate during slide transport (Posamentier, H. W. & Martinsen, O. J., 2011; Ortiz-Karpf, A. *et al.*, 2017; Hodgson, D. *et al.*, 2018; Sobiesiak, M. S. *et al.*, 2018). Based on their orthogonal relationship with the headwall scarp, these grooves are a reliable indicator of the translation pathway of the slide through the evacuation zone.

Upper translational domain

Description.– Grooves in the updip part of the upper translational domain (Fig. 7A) are the downdip continuation of those within the evacuation zone (see Fig. 6), displaying similar dimensions and geometries (see Headwall domain section). However, grooves in this domain converge downdip towards the NE lateral margin (Fig. 7A), which contrasts to the more commonly described downdip-diverging grooves (e.g. Posamentier, H. W. & Kolla, V., 2003; McGilvery, T. A. H., Geoffrey, 2004; Ortiz-Karpf, A. *et al.*, 2017). In the central part of the basal-shear surface is a pair of broadly NW-trending, slightly curved lineations that bound an area slightly elevated (*c.*10 m) compared to its surrounding area, and which mark subtle changes in the depth of the basal-shear surface (medium grey-shaded grey in Fig. 7A). Adjacent to the NE lateral margin is an area of highly discontinuous reflections, best expressed on the variance map in Fig. 7A. Within this area are lineations oriented oblique to the NE lateral margin. This area is also characterised by low-to-medium amplitude, discontinuous reflections at, and immediately beneath, the basal-shear surface (Fig. 7D). On top of the older slide, there are several 0.5-1.5 km-long lineations that connect to, and trend at *c.*45 ^{o} to, the NE lateral margin (Figs. 7A and D).

The proximal part of the upper translational domain is dominated by debrite (SF-1) that surrounds scattered megaclasts (SF-4) (Fig. 7B). These megaclasts have elliptical to rectangular planview geometries, with long-axis lengths ranging from *c.*0.18 to 1 km and thicknesses of *c.*70 to 140 m (Fig. 7B). Seismic sections show that these megaclasts are sometimes internally folded and faulted (Fig. 7D). Megaclasts are concentrated in the central part of this domain, where they form a *c.*15 km-long

and 3 km-wide, convex-updip cluster. This cluster is bound by a gradational boundary with SF-1 in the E, and an abrupt boundary in the W with Area B, the latter defined by the longitudinal shear zone across which they abruptly change their orientation from convex-updip to -downdip (Fig. 7B). Most of the megaclast cluster occurs within Area A, although another, seemingly smaller cluster is observed *c.*5 km downdip to the N within Area B (Fig. 7B), with the two being separated by the longitudinal shear zone. Immediately downdip of the Area A megaclast cluster are several convex-updip bands are developed within the slides debritic matrix (Fig. 7B) and that, critically, extend upwards through the slide and are expressed on its top surface, where they form positive relief at the seabed (Fig. 7C). It is also important to note that these bands are sub-parallel to the overall, convex-updip geometry of the cluster and to the long-axis of elongated clasts (Figs. 7B and 8A). In contrast, downdip from the eastern margin of the cluster, the bands show a convex-downdip geometry, terminating at the NE lateral margin (Figs. 7B and 8A). A NW-trending, narrow band (*c.*500 m-wide and *c.*10 km-long) of debrite (SF-1), which is possibly the expression of an intra-Area A shear zone, defines the boundary between these two sets of bands (Fig. 7B).

Interpretation.– The converging-downdip geometry of the grooves implies that the pathway of the slide was focused towards the steep, NE lateral margin (Fig. 7A). As a result, the slide is thickest adjacent to this margin (see Fig. 3A). The pathway was likely controlled by the morphology of the basal-shear surface that broadly follows the morphology of the underlying substrate (see Fig. 4B). This supports the observations of Ortiz-Karpf, A. *et al.* (2017), who provide evidence for the impact of seabed morphology on the emplacement of submarine landslides. We interpret the pair of curved lineations as 'ramps' bounding an area called a 'flat' (Fig. 7A) (Trincardi, F. & Argnani, A., 1990; Lucente, C. C. & Pini, G. A., 2003; Frey-Martinez, J. *et al.*, 2005; Bull, S. *et al.*, 2009). The ramps record basal erosion by the overlying slide that are commonly expressed by truncated reflections of underlying substrate by a basal-shear surface (e.g. Bull, S. *et al.*, 2009). However, as the ramps in this domain represent relatively small steps (i.e. 10 m), the basal-shear surface does not truncate more than one

reflection. We interpret the lineations oriented oblique to the NE lateral margin on, and immediately beneath, the basal-shear surface (Fig. 7A) as substrate that have undergone contractional deformation due to stress exerted by the passing slide, forming a 'basal-shear zone' (Butler, R. & McCaffrey, W., 2010; Hodgson, D. *et al.*, 2018; Cardona, S. *et al.*, 2020). Lineations on top of the older slide (Fig. 7A) are interpreted as shear fractures (i.e. Riedel shears) that developed due to dextral strike-slip movement along the NE lateral margin as the Gorgon Slide translated northwestwards (e.g. Fleming, R. W. & Johnson, A. M., 1989; Martinsen, O., 1994; Fossen, H., 2016) (Fig. 7A). Fleming, R. W. and Johnson, A. M. (1989) suggest that this type of fractures is developed during an early stage of strike-slip faulting along the lateral margin of the slides, prior to the formation of through-going lateral margins. They recorded fractures oriented at 45^{o} clockwise from the trend of a dextral lateral margin, like the shear fractures observed here.

The scattered megaclasts in the proximal part of this domain are clustered (see Fig. 7B), possibly due to downdip-convergence of material within the Gorgon Slide (see Fig. 7A). We suggest that the clusters of megaclasts in Areas A and B were initially emplaced as a single cluster that was subsequently cross-cut by the longitudinal shear zone (Figs. 7B and 8), with the formation and clustering of megaclasts possibly inducing intra-slide velocity perturbations and/or variable total strains. These perturbations are evidenced by across-strike variations in the attitude of flow fabrics, which we infer are formed due to intra-flow compression (cf. ‘pressure ridges’ or ‘secondary flow fabrics’ of Bull, S. *et al.* (2009)); i.e. convex-downdip flow fabrics in Areas A and B are located further downflow of the convex-updip flow fabrics preserved immediately downdip, and perhaps in the strain shadow zone of the megaclast cluster in Area A (Figs. 7B and 8). Another indicator of internal variations in intra-flow velocity and/or total strain is the narrow area within Area A that separates the convex-downdip and -updip flow fabrics (Fig. 7B). This area is interpreted as an ‘internal shear zone’ (cf. Ogata, K. *et al.*, 2014; Bull, S. & Cartwright, J. A., 2019; Omeru, T. & Cartwright, J. A., 2019) that contains disaggregated material due to intense shearing. Other studies have also discussed how the entrainment and abrasion of

megaclasts during slide emplacement could affect flow rheology (e.g. Joanne, C. *et al.*, 2013; Ortiz-Karpf, A. *et al.*, 2017; Hodgson, D. *et al.*, 2018; Sobiesiak, M. S. *et al.*, 2019), and therefore spatial variations in intra-slide flow velocity.

Lower translational domain

Description.– On the basal-shear surface, the majority of kinematic indicators observed in the upper translational domain extend downdip into the lower translational domain (i.e. the basal-shear surface ramp and its associated shear fractures; Fig. 9A). Grooves on the basal-shear surface are, however, absent, and we note that the ramps are deeper (*c.*20 m-deep, Fig. 9D) than in the upper translational domain, and lineations within the deformed substrate area are more apparent (Fig. 9A). Downdip from the deformed substrate are several SE-facing ramps (i.e. perpendicular to transport direction) that merge updip with the ramp extending downdip from the upper translational domain (Fig. 9A). NE of the deformed substrate, beyond the lateral margin and on top of the older slide, are the downdip continuation of the N-trending shear fractures seen in the upper translational domain. These fractures die-out downdip to the N.

The convex-updip intra-flow fabric, bound between the longitudinal and internal shear zones within Area A, and which extends vertically through the deposit such that it is expressed on its top surface, dies-out downdip (Fig. 9B). In contrast, the convex-downdip flow fabrics within Area B continue and are in fact more prominent in this lower translational domain (Fig. 9B). Adjacent to the NE lateral margin is another cluster of megaclasts (Fig. 9B). In cross-section (Fig. 9D), this cluster contains megaclasts that have similar seismic expression to those in the upper translational domain (Figs. 7D and 8B-C). However, these megaclasts have shorter long-axes (*c.*0.05 to 0.54 km-long, compared to *c.*0.17 to 0.98 km-long) and are thicker (*c.*73 to 220 m, compared to *c.*70 to 137 m-thick) than those in the upper translational domain (see Fig. 10A). The long-axes trends of megaclasts in the upper (NNW) and lower (NE) translation domains also differ (Fig. 10B).

303 The internal shear zone (within Area A) merges with the longitudinal shear zone (defining the
304 boundary between areas A and B) in the distal part of the lower translational domain (Fig. 9C). These
305 shear zones outline a downdip-narrowing area defined by broadly convex-updip ridges. Consequently,
306 Area A becomes dominated by the convex-downdip ridges (Fig. 9C). However, immediately downdip
307 from the point where the shear zones merge, the ridges in Area A have slightly convex-updip
308 geometries, most notably adjacent to the longitudinal shear zone (Fig. 9C).

309 **Interpretation.–** The ramps, deformed substrate, and shear fractures indicate that seabed erosion and
310 deformation also occurred in this lower translational domain (Fig. 9A). The continuation of the
311 longitudinal and internal shear zones suggests that the related intra-flow velocity variation identified
312 in the upper translational domain also characterized the lower translational domain (Fig. 9B). Critically,
313 however, the gradual downflow disappearance of the convex-updip flow fabrics between these shear
314 zones suggests a downflow decrease in the internal velocity perturbations and/or total strains induced
315 by the cluster of megaclasts in the upper translational domain (Fig. 7B).

316 The cluster of megaclasts adjacent to the NE lateral margin (Figs. 9B and D) is located immediately
317 downflow from, and has a similar width (2.5 km) to, the deformed substrate area (Fig. 9A). Similar to
318 the observation from the Rapanui MTD (Cardona, S. *et al.*, 2020), where the presence of deformed
319 substrate could be correlated to higher concentrations of rafted blocks (i.e. megaclasts). The higher
320 concentration of megaclasts indicates an increase in flow competence overriding the area of the
321 deformed substrate. In addition, the long-axis orientations of the megaclasts in the lower translational
322 domain are generally oblique-to-sub-parallel to the overall north-westerly transport direction, which
323 contrasts to those in the upper translational domain that are generally perpendicular to the transport
324 direction (Fig. 10B). Their long-axis orientations are likely to be controlled by velocity gradients
325 (Mazzanti, P. & De Blasio, F., 2010), where the megaclasts in the lower translational domain, adjacent
326 to the NE lateral margin, were dragged against the stationary lateral wall (Fig. 9B). In contrast, the
327 cluster of megaclasts in the upper translational domain, further away from the lateral margin,

328 experienced a lower across-strike velocity gradient, meaning their long axis formed an overall convex-
329 updip geometry (Fig. 7B).

330 The top surface supports the interpretation of kinematic indicators within the internal body of the
331 slide (Figs. 9B-C). Here, it is also evident that velocity perturbation induced by the cluster of megaclasts
332 in upper translational domain (Figs. 7B and 8A) had decreased, and diminished downdip, as clearly
333 marked by the merging of the two shear zones (Fig. 9C). However, downdip from the point where
334 these two merges, the presence of convex-updip ridges within Area A (terminating at the longitudinal
335 shear zone) suggests that internal velocity perturbations continued (Fig. 9C).

336 *Toe domain*

337 **Description.–** The basal-shear surface in this domain serves as the frontal margin of Area A, and swings
338 through 90^{o} to join the lateral margin of Area B, which that continues downdip, beyond the area
339 imaged by 3D seismic reflection data (Fig. 11A). The seismic attribute expression of the deformed
340 substrate (Fig. 11A) resembles that of the upper and lower translational domains, being characterized
341 by high variance values (see Figs. 7A and 9A). In the SW part of this domain, there is a *c.*30 m-high
342 ramp (Figs. 10A and D), which is of higher-relief than the one developed updip in the lower
343 translational domain (*c.*20 m).

344 Debrite (SF-1) and a fold-and-thrusts system (SF-3) dominate the distal part of Area A and B in the toe
345 domain, respectively (Fig. 11B). The thrusts within Area B dip to the SE, sub-parallel to the transport
346 direction of the slide (see Figs. 5G, 11B and D). Within the older slide, there is a cluster of relatively
347 large megaclasts (*c.*2.5 km-wide and *c.*5 km-long) that are deformed by NNW-SSE-striking, NE-dipping
348 thrusts; these trend broadly perpendicular Area A's frontal margin and the NW-SE-striking thrusts
349 within Area B (see Fig. 11B). We note that a relatively small number of these thrusted megaclasts (i.e.,
350 indicated by high RMS amplitude and brown colour in Fig. 11B) are observed within the very frontal
351 part of Area A, where they are encased in debrite (green colour in Fig. 11B). The thrusts within

megaclasts in Area A (i.e., NW-SE-to-E-W) have more variable strikes than those in the older slide (i.e., consistently NW-SE) (Fig. 11B). We also note that thrusts within the older slide and Area A are unidirectional, whereas those in Area B form pop-up-bounding conjugate pairs (Fig. 11B and D). The toe region of Area A is defined by a rugose seabed characterized by *c.*30 m-high ridges that are elevated above the flat seabed capping the older slide (see Fig. 11C). The vertical relief of the ridges in Area A is higher than in both Area B (*c.*10 m, Fig. 11C) and the lower translational domain (*c.*10 m, Fig. 9).

Interpretation.– The presence of a ramp along the basal-shear surface, which caps deformed substrate material, indicate that substrate deformation and erosion continued beneath the main body of the slide, even in this relatively distal location. Critically: (i) the abrupt truncation of most of the thrusted megaclasts in the older slide by the frontal margin of Area A; (ii) the strike difference between thrusts within areas A and B and those in the older slide (Fig. 11B); and (iii) the structural style difference between the thrusts in Area B, and Area A and the older slide indicate that most of the thrusted megaclasts belong to a slide deposited prior to the emplacement of the Gorgon Slide. However, the fact that a relatively small number of thrusted megaclasts are present in the very frontal part of Area A (Fig. 11B) suggest local cannibalization of the older slide by the Gorgon Slide.

Another key observation is that Area B extends further downdip than Area A (Fig. 11A) and that the longitudinal shear zone extends from the upper translational domain (see Figs. 7A and 8A) to join Area B's lateral margin in the toe domain (Fig. 11B). This may indicate an effect frontal margins of the cells on inferred intra-slide velocity perturbation. Specifically, the velocity perturbation could have originated due to the passage of the Gorgon Slide onto (i.e. Area A), and partly around (i.e. Area B), frontal confinement of Cell A, with this perturbation and subsequent arrest of the flow in Area A propagating upflow (Fig. 11B). Therefore, this velocity perturbation may have connected with the downflow-propagating velocity perturbation induced by the cluster of megaclasts in the upper translational domain (Figs. 7B and 8A). The frontal confinement of Cell A is likely to be controlled by

the depth of basal-shear surface that is deeper than that of the Cell B. Moernaut, J. and De Batist, M. (2011) suggest that the depth of the basal shear surface is a key control on frontal emplacement style (frontally confined versus emergence, sensu Frey-Martínez, J. *et al.*, 2006). A deeper basal shear surface implies a higher potential-energy threshold that must be exceeded for the moving mass to abandon the basa-shear surface and emerge onto the coeval basin floor, thereby favouring frontal confinement. In contrast, a shallower basal-shear surface lowers this threshold, making frontal emergence more likely.

Emplacement processes of the Gorgon Slide: a multi-cell flow emplacement mechanism

Single versus multiple failure events.– *Was the Gorgon Slide deposited during a single event, or does it comprise multiple, stacked deposits, emplaced by several, temporally discrete events?* Establishing this is key to developing a kinematic model for slide emplacement, and for assessing the potential geohazard potential of the related flows. Such stacked deposits might be anticipated in the Cenozoic stratigraphy of the NW Shelf of Australia, given it is characterised by repeated slope failures (Hengesh, J. V. *et al.*, 2013; Nugraha, H. D. *et al.*, 2019; Wu, N. *et al.*, 2026). We acknowledge that answering these related questions is not straightforward, given our lack of borehole data and the still relatively limited resolution (8-11 m) of even these high-quality 3D seismic reflection data. For example, individual gravity-flow deposits, and/or thin pelagic or hemipelagic intervals separating them, could be thinner than the resolution of our seismic reflection data.

We therefore attempt to answer these questions using the following criteria: (i) *does the slide source area contain evidence for multiple slope failure events?* – we note that the headwall scarp of the slide is relatively simple, being defined by a single, relatively smooth, downdip-facing plane, readily explainable as forming during a single slope failure event, rather than by a composite staircase-like geometry that might reflect punctuated, retrogressive failure of the slope (e.g., Sawyer, D. E. *et al.*, 2009). We observe crown cracks immediately updip of the main scarp; these possibly mark the location of future slope failure events, which ultimately would give rise to a staircase-like scarp

geometry (Varnes, D. J., 1978; Frey-Martinez, J. *et al.*, 2005); (ii) *does the basal-shear surface containing evidence for temporally separate, but spatially related flows?* - we observe downdip converging grooves on the basal-shear surface immediately downdip of the slide headwall (Fig. 6) and in the upper translational domain (Fig. 7A). These grooves do *not* cross-cut one another (cf. Wu, N. *et al.*, 2026), suggesting they formed during a single event (e.g., Scarselli, N. *et al.*, 2013). We note that we see *no evidence* for intra-slide basal-shear surfaces decorated by grooves; (iii) *is there evidence for stratigraphically discrete deposits defined by their own distinct structural style?* - within the upper and lower translational domains, and the toe domain, we note that the shear zones (e.g. Figs. 5D-E), thrusts (e.g. Fig. 5G), flow fabrics (e.g., Figs. 7B-C and 9B-C), and megaclasts (Fig. 8B) span the entire height of the slide, being observable on broadly stratigraphically concordant maps generated within the deposits, as well as at the top of the deposit, i.e., these features are through-going and *not* stratigraphically decoupled; (iv) *is there any evidence for relatively continuous, through-going, intra-slide fine-grained (e.g., pelagic, hemipelagic) deposits separating individual sediment gravity-flow deposits (e.g., mass-transport deposits)?* - across the deposit and at the scale of resolution afforded to us by our seismic reflection data, we see no (seismically resolvable) evidence for intra-deposit hemipelagic (or similar) deposits that might represent even brief hiatuses between more rapid, catastrophic, slide-related deposition. However, we confidently infer such deposits capping the slide overlain and eroded into by the Gorgon Slide, suggesting a relatively long period between the deposition of the these two units (e.g. Fig. 4B); and (v) *does the lateral margin contain evidence for formation by multiple slope failure events?* – the lateral margin is geometrically similar to the headwall, i.e., it is defined by a structurally simple, sub-vertical plane that can be mapped continuously over a remarkably long distance (i.e., c.30 km), suggesting it too formed during a single event (e.g. Fig. 3B).

Given these observations, our preferred interpretation is that the Gorgon Slide was emplaced during a single event. Deposition of such a large slide (i.e., total volume of *c.*500 km^3, with a thickness of up to 500 m) by a single event is not unusual, with similar features described from offshore New Zealand

(Joanne, C. *et al.*, 2013), South China Sea (Sun, Q. *et al.*, 2018b), and offshore Brunei (Gee, M. *et al.*, 2007).

A multi-cell emplacement model.– A multiple flow cell model for subaqueous slides is proposed by Alsop, G. I. and Marco, S. (2014) based on field data, developing a model originally proposed by Farrell, S. G. (1984). They suggest that a large (first-order) slide consists of a number of smaller (second-order) flow cells formed during the transport and ultimate emplacement of a sediment mass. These smaller flow cells may interact with each other and cause overprinting on earlier formed structures. Similar kinematic interactions between intra-flow cells are documented from sonar (e.g., Prior, D. B. *et al.*, 1984; Masson, D. *et al.*, 1993; Gee, M. J. *et al.*, 2001) and 3D seismic reflection data (e.g., Bull, S. *et al.*, 2009; Steventon, M. J. *et al.*, 2019; Nugraha, H. D. *et al.*, 2020; Abu, C. *et al.*, 2022), where primary (longitudinal shear zone) and secondary (sinuous) flow fabrics form between and define evolving cells (sensu Bull, S. *et al.*, 2009). These kinematic indicators suggest the portions (i.e. cells) of the translating mass were travelling at different speeds and/or travelled at slightly different times (Masson, D. *et al.*, 1993; Gee, M. *et al.*, 2005).

In this study, the Gorgon Slide appears to comprise at least two intra-slide (second-order) flow cells. These are represented physically by Areas A and B, and for the purpose of this process-based interpretation are re-named as Cells A and B, respectively. The emplacement processes of the Gorgon Slide are captured in a schematic model that recognises three stages of development (Fig. 12).

Stage 1.– Prior to slope degradation, a surface rupture might have been triggered by two main mechanisms (Fig. 12A). First, the normal faults bounding the horst could have been inverted due to regional compression, which then destabilised the slope (Keep, M. *et al.*, 1998; Nugraha, H. D. *et al.*, 2019). Second, the existence of pockmarks observed on the seabed (see Fig. 6) implies that there has been active fluid venting in the headwall area (Hengesh, J. V. *et al.*, 2013), most likely originating from the underlying, gas-bearing horst block (Fig. 2). Gas leakage into shallower sediments could have

lowered the shear strength of these sediments, and primed the slope for subsequent failure (Scarselli, N. *et al.*, 2013). However, the Gorgon Slide was not an isolated occurrence, but rather the most recent. Previous collapse of the continental margin is recorded in the older (pre-Gorgon) slide (see Fig. 4).

Stage 2.–The arcuate geometry of the main headwall scarp indicates that the failed sediments were evacuated during a single landslide event (see Fig. 6). The evacuated sediments might include megaclasts derived from either the headwall and/or megaclasts entrained from the layered slope substrate. During translation, the megaclasts were deformed and fragmented (e.g., Nwoko, J. *et al.*, 2020). The downdip-converging grooves within the headwall and upper translational domains suggest a convergent pathway of the slide, resulting in the clustering of the megaclasts (Fig. 12B). In the lee-side of the cluster of megaclasts, the following features formed: (i) convex-updip flow fabrics within the slide, and (ii) convex-updip ridges on top of the slide. These features indicate slower transport velocity in and around the area of concentrated megaclasts (Fig. 12B). Higher transport velocities of flows moving around the megaclast-rich area led to the formation of the longitudinal shear zone, and the initiation of Cells A and B. The cluster of megaclasts effectively acted as an obstacle to the initial, single-cell flow. Other studies have also documented such mechanism, where the geometry of flow fabrics and ridges downdip from translating megaclasts suggest slower-moving flows than surrounding materials (e.g., Masson, D. *et al.*, 1993; Lastras, G. *et al.*, 2005; Gee, M. *et al.*, 2006; Bull, S. *et al.*, 2009).

Stage 3.– The downdip propagation of the basal-shear surface was coupled with the evolution of the internal body and top surface of the slide. The area covering the convex-updip flow fabrics and ridges narrowed downdip (Fig. 12C), which suggests a reduction in the influence of the cluster of megaclasts on slowing down the flow of material in its lee-side. Thus, we interpret this area as a 'shadow zone'. The shadow zone is bound by the longitudinal shear zone separating the two cells, and the internal shear zone within Cell A (Fig. 12C). The formation of this shadow zone and related bounding structures

475 illustrates how megaclasts influence flow processes within a slide (e.g. Masson, D. *et al.*, 1993;
476 Lucente, C. C. & Pini, G. A., 2003; Jackson, C. A., 2011; Hodgson, D. *et al.*, 2018).

477 Downdip from the shadow zone, ridges within Cell A show convex-updip geometries adjacent to the
478 longitudinal shear zone. In contrast, ridges within Cell B consistently exhibit convex-downdip
479 geometries (Fig. 12C). These geometries indicate that Cell A resisted the downdip translation of Cell
480 B, meaning its internal ridges were dragged downdip whereas those in Cell B were dragged updip (Fig.
481 12C). Therefore, we suggest that Cell A was travelling more slowly than Cell B. Furthermore, the
482 prominent seabed relief characterizing the frontal margin of Cell A suggest a shortening and thickening
483 effect driven by this part of the flow being frontally confined (Fig. 12C) (Masson, D. *et al.*, 1993; Gee,
484 M. *et al.*, 2006). Cell B, however, was able to translate further downdip than Cell A, meaning the
485 former travelled faster and further than the latter.

486 **DISCUSSION**

487 *Impact of flow cell formation on submarine landslide kinematics and structure*

488 Submarine debris flows can travel for tens to hundreds of km across low gradient (*c.*<1^{o}) continental
489 slopes, despite their cohesive nature (Gee, M. *et al.*, 1999; Lastras, G. *et al.*, 2005). This mobility can
490 be explained by sustained pore-fluid pressure within the flow during transport (Major, J. J. & Iverson,
491 R. M., 1999; McArdell, B. W. *et al.*, 2007), and the presence of a thin lubricating layer of fluid at the
492 base of the frontal part of the flow (i.e. hydroplaning, Mohrig, D. *et al.*, 1998). Ultimately, a debrite is
493 formed by *en masse* freezing of the debris flow (e.g. Talling, P. J. *et al.*, 2012), where materials at flow
494 margins (i.e. frontal and lateral) cease moving first, followed by materials in the main body of the flow
495 (Iverson, R. M., 1997).

496 The Gorgon Slide provides evidence of a mass flow splitting into two smaller flow cells (Cell A and B,
497 Fig. 12). The relationship between the two cells suggests that Cell A ceased movement, while Cell B
498 was still in motion. This suggests that *en masse* freezing did not occur across the entire body of the

499 flow synchronously. Instead, individual flow cells froze at different times, resulting in different runout
500 duration and distance of the cells. We propose that lateral friction and related pore-fluid pressure
501 played an important role in controlling the runout distance of the two cells, in addition to the frontal
502 confinement. The longitudinal shear zone may have sustained excess pore-fluid pressure between the
503 two cells, such that low friction between the two cells could be maintained, allowing continued
504 translation of Cell B despite being partly impeded by Cell A. In contrast, pore-fluid pressure was likely
505 dissipated at the lateral margins of the flow during translation (e.g. NE lateral margin, Fig. 3), resulting
506 in relatively high friction between the moving slide (e.g. Cell A) and stationary lateral substrate (i.e.
507 the older slide and locally other slope strata). This high friction at the lateral margin was likely to
508 reduce runout distance more significantly than the friction at the longitudinal shear zone. Such
509 mechanisms are also observed from experimental studies (Major, J. J. & Iverson, R. M., 1999; De Haas,
510 T. *et al.*, 2015). Our results suggest that a multi-cell debris flow could undergo 'punctuated' freezing,
511 where one cell may have a shorter runout distance than the others due to spatial differences in the
512 pore pressure and related friction between bounding cells.

513 *Controls on flow cell formation*

514 Flow cell formation within a slide depends on internal velocity perturbations, which are controlled by
515 variations in at least three local factors (Farrell, S. G., 1984; Alsop, G. I. & Marco, S., 2011; 2014): (i)
516 the lithology and/or geometry of stratigraphic elements overridden by the slide (e.g. older slides,
517 channels and lobes); (ii) fluid pressures within the slide and/or its substrate and lateral margins; and
518 (iii) the slope gradient and/or geometry of basal-shear surface underlying the slide.

519 In the Gorgon Slide, a cluster of megaclasts within a debritic matrix-initiated flow cell formation. This
520 implies that lithology, in particular variations of the degree of disaggregation within the slide, play a
521 key role in forming the two seismic-scale flow cells. Variability of local fluid pressures within the slide
522 could be represented by the interactions between the slide and clustered megaclasts in the upper

translational domain (e.g., Figs. 7B and 12B). As an obstacle to flow, the clustered megaclasts may increase local fluid pressure as they resisted the translating slide, and thus induce the formation of the cells. In addition, the geometry of the basal-shear surface was also important, given it caused the flow to converge, clustering the megaclasts, initiating velocity perturbation, and terminating the flow cells. Most notably, frontal confinement of Cell A, along with the high-relief top surface, coincides with deeper basal-shear surface as compared to those of Cell B that has shallower basal-shear surface (see Fig. 4B). As demonstrated by (Moernaut, J. & De Batist, M., 2011), the depth of the basal shear surface exerts a key control on the frontal margin of a slide: a deeper basal-shear surface may be associated with frontal confinement, whereas a shallower basal-shear surface may be associated with frontal emergence. By having laterally different depth of basal-shear surface, a single slide event could therefore display both frontal confiment and emergence along its toewall, for example, along the toewall of the Haya Slide in the Makassar Strait, Indonesia (Nugraha, H. D. *et al.*, 2020).

Local variations of lithology, fluid pressure and basal-shear surface geometry may have been influential prior to emplacement, but their properties could also evolve during translation and cessation of the parent flow (Iverson, R. M., 1997; Dykstra, M. *et al.*, 2011; Joanne, C. *et al.*, 2013; Alsop, G. I. & Marco, S., 2014; Ortiz-Karpf, A. *et al.*, 2017; Hodgson, D. *et al.*, 2018).

Implications for geohazard risk assessment

Submarine landslide emplacement can severely damage seabed infrastructure, including submarine pipelines (Parker, E. J. *et al.*, 2008; Zakeri, A., 2009; Randolph, M. F. & White, D. J., 2012; Vanneste, M. *et al.*, 2013). A key control on pipeline survivability is the drag imposed by the moving mass flow, which can determine whether a pipeline remains in place or is torn out and transported downslope (Parker, E. J. *et al.*, 2008; Zakeri, A., 2009). Quantifying this drag is therefore a critical requirement in the design of seafloor installations (e.g., Zakeri, A., 2009). The translation of distinct flow cells, such as Cells A and B, suggests that, even within a single slide, pipelines may be subjected to two mass flows with differing

rheology and transport velocity. This could produce spatially variable drag forces and, along the longitudinal shear zone, intensified shearing may further elevate the likelihood of pipeline failure. Accordingly, the flow behaviour recorded in the Gorgon Slide provides useful constraints for experimental (e.g., Zakeri, A. *et al.*, 2008) and numerical (e.g., Zakeri, A., 2009; Randolph, M. F. & White, D. J., 2012) modelling.

CONCLUSIONS

This interpretation of a 3D seismic reflection dataset, investigating the emplacement of a recent submarine landslide, the Gorgon Slide (Exmouth Plateau, offshore NW Australia), concludes that:

1. The Gorgon Slide was evacuated from a steep, NE-SW trending, *c.*350 m-high headwall scarp and transported towards the NW. Layered slope strata in this headwall domain are the likely source of megaclasts that are subsequently transported downdip.
2. In the proximal part of the translation domain, downdip-converging grooves on the basal-shear surface indicate that the pathway of the slide was focused towards its lateral margin in the NE. The convergent pathway of the flow results in the clustering of the megaclasts, whose long-axes are generally trending NE-SW, perpendicular to the transport direction. This clustering of megaclasts became an obstacle to flow, causing velocity perturbation within the slide. The velocity perturbation is recorded by convex-updip flow fabrics within the internal body, and by convex-updip ridges on the seabed. These features indicate a slower transport velocity of the cluster of megaclasts and materials in its lee-side. The area of the slower-moving material narrows downdip, indicating that velocity perturbation caused by the cluster of megaclasts gradually diminished downflow, forming a ‘shadow zone’. Transport velocities of flows were higher around the megaclasts, resulting in the formation of longitudinal shear zones and the initiation of two flow cells, namely Cells A and B.
3. The distal part of the translation domain contains kinematic indicators recording erosional and deformational processes on the basal-shear surface. Erosional processes are evidenced

by a ramp, and deformational processes are evidenced by deformed substrate or basal-shear zone and shear fractures adjacent to the NE lateral margin. The deformed substrate and shear fractures are closely related to the thickest part of the slide, comprising a cluster of megaclasts, with individual megaclasts generally trending NNW-SSE, oblique to sub-parallel to the transport direction. Flow fabrics within the slide and ridges on the seabed of Cell A were dragged downdip, while those of Cell B were dragged updip. This points to Cell A acting as an impediment to the movement of the faster-moving Cell B.

4. In the toe domain, the frontal margin of Cell A is marked by positive seabed relief (*c.*30 m-high) that gradually decreases updip, which is significantly higher than the relief of Cell B (*c.*10 m-high). This suggests that Cell A was buttressed against its frontally-confined toewall that coincides with a pre-existing cluster of megaclasts (i.e. encased by older slide) and deeper basal-shear surface, while Cell B was not. Therefore, as there were no flow obstacles, Cell B was able to travel further than Cell A.
5. The morphology of the basal-shear surface and the degree of disaggregation within the slide, especially the megaclasts, played important roles in flow cell evolution. The basal-shear surface controlled the pathway of the slide, and the clustering of the megaclasts. The megaclast clusters induced internal velocity perturbations that controlled the initiation and cessation of intra-slide flow cells.
6. Simultaneous *en masse* freezing was unlikely to have occurred throughout the body of the Gorgon Slide. Instead, 'punctuated' freezing, where motion in Cell A had ceased while Cell B was still active, occurred due to differential friction and pore-fluid pressure dissipation at flow cells margins. For instance, excess pore-fluid can be maintained within the longitudinal shear zone, so that Cell B only experienced minimal friction against the Cell A. In contrast, excess pore-fluid pressure was likely to dissipate at lateral margins, such as at the NE lateral margin separating Cell A and stationary substrate. Thus, Cell A experienced higher lateral friction than

that of Cell B, resulting in reduced runout distance. This punctuated freezing mechanism may be considered for modelling the impact of submarine landslides on submarine infrastructures.

ACKNOWLEDGEMENTS

We thank Geoscience Australia for providing seismic and borehole data. Schlumberger and Geoteric are thanked for providing software academic license.

CONFLICT OF INTEREST

No conflict of interest declared.

REFERENCES

ABU, C., JACKSON, C.A.-L. & FRANCIS, M. (2022) Strike-Slip Overprinting of Initial Co-Axial Shortening within the Toe Region of a Submarine Landslide and a Model for Basal Shear Surface Growth: A Case Study from the Angoche Basin, Offshore Mozambique. *Journal of the Geological Society*, **179,** jgs2021-2032.

ALSOP, G.I. & MARCO, S. (2011) Soft-Sediment Deformation within Seismogenic Slumps of the Dead Sea Basin. *Journal of Structural Geology*, **33,** 433-457.

ALSOP, G.I. & MARCO, S. (2014) Fold and Fabric Relationships in Temporally and Spatially Evolving Slump Systems: A Multi-Cell Flow Model. *Journal of Structural Geology*, **63,** 27-49.

ALVES, T.M., KURTEV, K., MOORE, G.F. & STRASSER, M. (2014) Assessing the Internal Character, Reservoir Potential, and Seal Competence of Mass-Transport Deposits Using Seismic Texture: A Geophysical and Petrophysical Approach. *AAPG Bulletin*, **98,** 793-824.

APTHORPE, M. (1988) Cainozoic Depositional History of the North West Shelf. *The North West Shelf, Australia: Petroleum Exploration Society of Australia***,** 55-84.

BOYD, R., WILLIAMSON, P. & HAQ, B. (1993) Seismic Stratigraphy and Passive-Margin Evolution of the Southern Exmouth Plateau. *Sequence Stratigraphy and Facies Associations***,** 579-603.

BROWN, A.R. (2011) *Interpretation of Three-Dimensional Seismic Data*. The American Association of Petroleum Geologists and the Society of Exploration Geophysicists, Tulsa.

BULL, S., CARTWRIGHT, J. & HUUSE, M. (2009) A Review of Kinematic Indicators from Mass-Transport Complexes Using 3d Seismic Data. *Marine and Petroleum Geology*, **26,** 1132-1151.

BULL, S. & CARTWRIGHT, J.A. (2019) Line Length Balancing to Evaluate Multi-Phase Submarine Landslide Development: An Example from the Storegga Slide, Norway. *Geological Society, London, Special Publications*, **500**.

BUTLER, R. & MCCAFFREY, W. (2010) Structural Evolution and Sediment Entrainment in Mass-Transport Complexes: Outcrop Studies from Italy. *Journal of the Geological Society*, **167,** 617-631.

CARDONA, S., WOOD, L.J., DUGAN, B., JOBE, Z. & STRACHAN, L.J. (2020) Characterization of the Rapanui Mass-Transport Deposit and the Basal Shear Zone: Mount Messenger Formation, Taranaki Basin, New Zealand. *Sedimentology*.

CATHRO, D.L., AUSTIN JR, J.A. & MOSS, G.D. (2003) Progradation Along a Deeply Submerged Oligocenemiocene Heterozoan Carbonate Shelf: How Sensitive Are Clinoforms to Sea Level Variations? *AAPG bulletin*, **87,** 1547-1574.

CHOPRA, S. & MARFURT, K.J. (2007) *Seismic Attributes for Prospect Identification and Reservoir Characterization*. Society of Exploration Geophysicists Tulsa, Oklahoma.

DE HAAS, T., BRAAT, L., LEUVEN, J.R., LOKHORST, I.R. & KLEINHANS, M.G. (2015) Effects of Debris Flow Composition on Runout, Depositional Mechanisms, and Deposit Morphology in Laboratory Experiments. *Journal of Geophysical Research: Earth Surface*, **120,** 1949-1972.

DOTT, R. (1963) Dynamics of Subaqueous Gravity Depositional Processes. *AAPG Bulletin*, **47,** 104-128.

DYKSTRA, M., GARYFALOU, K., KERTZNUS, V., KNELLER, B., MILANA, J.P., MOLINARO, M., SZUMAN, M. & THOMPSON, P. (2011) Mass-Transport Deposits: Combining Outcrop Studies and Seismic Forward Modeling to Understand Lithofacies Distributions, Deformations, and Their Seismic Stratigraphic Expression. *SEPM Special Publication*, **96,** 293-310.

ECKERSLEY, A.J., LOWELL, J. & SZAFIAN, P. (2018) High-Definition Frequency Decomposition. *Geophysical Prospecting*, **66,** 1138-1143.

FARRELL, S.G. (1984) A Dislocation Model Applied to Slump Structures, Ainsa Basin, South Central Pyrenees. *Journal of Structural Geology*, **6,** 727-736.

FISHER, R.V. (1983) Flow Transformations in Sediment Gravity Flows. *Geology*, **11,** 273-274.

FLEMING, R.W. & JOHNSON, A.M. (1989) Structures Associated with Strike-Slip Faults That Bound Landslide Elements. *Engineering Geology*, **27,** 39-114.

FOSSEN, H. (2016) *Structural Geology*. Cambridge University Press.

FREY-MARTINEZ, J., CARTWRIGHT, J. & HALL, B. (2005) 3d Seismic Interpretation of Slump Complexes: Examples from the Continental Margin of Israel. *Basin Research*, **17,** 83-108.

FREY-MARTÍNEZ, J., CARTWRIGHT, J. & JAMES, D. (2006) Frontally Confined Versus Frontally Emergent Submarine Landslides: A 3d Seismic Characterisation. *Marine and Petroleum Geology*, **23,** 585-604.

GEE, M., MASSON, D., WATTS, A. & ALLEN, P. (1999) The Saharan Debris Flow: An Insight into the Mechanics of Long Runout Submarine Debris Flows. *Sedimentology*, **46,** 317-335.

GEE, M., GAWTHORPE, R. & FRIEDMANN, J. (2005) Giant Striations at the Base of a Submarine Landslide. *Marine Geology*, **214,** 287-294.

GEE, M., GAWTHORPE, R. & FRIEDMANN, S. (2006) Triggering and Evolution of a Giant Submarine Landslide, Offshore Angola, Revealed by 3d Seismic Stratigraphy and Geomorphology. *Journal of Sedimentary Research*, **76,** 9-19.

GEE, M., UY, H., WARREN, J., MORLEY, C. & LAMBIASE, J. (2007) The Brunei Slide: A Giant Submarine Landslide on the North West Borneo Margin Revealed by 3d Seismic Data. *Marine Geology*, **246,** 9-23.

GEE, M.J., MASSON, D.G., WATTS, A.B. & MITCHELL, N.C. (2001) Passage of Debris Flows and Turbidity Currents through a Topographic Constriction: Seafloor Erosion and Deflection of Flow Pathways. *Sedimentology*, **48,** 1389-1409.

HENGESH, J.V., DIRSTEIN, J.K. & STANLEY, A.J. (2013) Landslide Geomorphology Along the Exmouth Plateau Continental Margin, North West Shelf, Australia. *Australian Geomechanics*, **48,** 71-92.

HODGSON, D., BROOKS, H., ORTIZ-KARPF, A., SPYCHALA, Y., LEE, D. & JACKSON, C.-L. (2018) Entrainment and Abrasion of Megaclasts During Submarine Landsliding and Their Impact on Flow Behaviour. *Geological Society, London, Special Publications*, **477,** SP477. 426.

HULL, J.N.F. & GRIFFITHS, C.M. (2002). *Sequence Stratigraphic Evolution of the Albian to Recent Section of the Dampier Sub-Basin, Northwest Shelf, Australia*. The Sedimentary Basins of Western Australia 3: Proceedings of the Petroleum Exploration Society of Australia Symposium, Perth.

IVERSON, R.M. (1997) The Physics of Debris Flows. *Reviews of geophysics*, **35,** 245-296.

JACKSON, C.A. (2011) Three-Dimensional Seismic Analysis of Megaclast Deformation within a Mass Transport Deposit; Implications for Debris Flow Kinematics. *Geology*, **39,** 203-206.

JOANNE, C., LAMARCHE, G. & COLLOT, J.Y. (2013) Dynamics of Giant Mass Transport in Deep Submarine Environments: The Matakaoa Debris Flow, New Zealand. *Basin Research*, **25,** 471-488.

KEEP, M., POWELL, C. & BAILLIE, P. (1998) Neogene Deformation of the North West Shelf, Australia. *The sedimentary basins of Western Australia*, **2,** 81-91.

LASTRAS, G., DE BLASIO, F.V., CANALS, M. & ELVERHØI, A. (2005) Conceptual and Numerical Modeling of the Big'95 Debris Flow, Western Mediterranean Sea. *Journal of Sedimentary Research*, **75,** 784-797.

LONGLEY, I.M., BUESSENSCHUETT, C., CLYDSDALE, L., CUBITT, C.J., DAVIS, R.C., JOHNSON, M.K., MARSHALL, N.M., MURRAY, A.P., SOMERVILLE, R. & SPRY, T.B. (2002) The North West Shelf of Australia - a Woodside Perspective. *The Sedimentary Basins of Western Australia 3: Petroleum Exploration Society of Australia Symposium*. M. Keep & S. J. Moss. Perth**,** 28-88.

LUCENTE, C.C. & PINI, G.A. (2003) Anatomy and Emplacement Mechanism of a Large Submarine Slide within a Miocene Foredeep in the Northern Apennines, Italy: A Field Perspective. *American Journal of Science*, **303,** 565-602.

MAJOR, J.J. & IVERSON, R.M. (1999) Debris-Flow Deposition: Effects of Pore-Fluid Pressure and Friction Concentrated at Flow Margins. *Geological Society of America Bulletin*, **111,** 1424-1434.

MARTINSEN, O. (1994) Mass Movements. In: *The Geological Deformation of Sediments* (Ed. by, 127-165. Springer.

MASSON, D., HUGGETT, Q. & BRUNSDEN, D. (1993) The Surface Texture of the Saharan Debris Flow Deposit and Some Speculations on Submarine Debris Flow Processes. *Sedimentology*, **40,** 583-598.

MASSON, D., HARBITZ, C., WYNN, R., PEDERSEN, G. & LØVHOLT, F. (2006) Submarine Landslides: Processes, Triggers and Hazard Prediction. *Philosophical Transactions of the Royal Society A: Mathematical, Physical and Engineering Sciences*, **364,** 2009-2039.

MAZZANTI, P. & DE BLASIO, F. (2010) Peculiar Morphologies of Subaqueous Landslide Deposits and Their Relationship to Flow Dynamics. In: *Submarine Mass Movements and Their Consequences* (Ed. by, 141-151. Springer.

MCARDELL, B.W., BARTELT, P. & KOWALSKI, J. (2007) Field Observations of Basal Forces and Fluid Pore Pressure in a Debris Flow. *Geophysical research letters*, **34**.

MCCORMACK, K. & MCCLAY, K. (2013). *Structural Architecture of the Gorgon Platform, North West Shelf, Australia*. The Sedimentary Basins of Western Australia IV: Proceedings of the Petroleum Exploration Society of Australia Symposium, Perth, WA.

MCGILVERY, T.A.H., GEOFFREY (2004) Seafloor and Shallow Subsurface Examples of Mass Transport Complexes, Offshore Brunei. *Offshore Technology Conference*. Houston.

MOERNAUT, J. & DE BATIST, M. (2011) Frontal Emplacement and Mobility of Sublacustrine Landslides: Results from Morphometric and Seismostratigraphic Analysis. *Marine Geology*, **285,** 29-45.

MOHRIG, D., ELLIS, C., PARKER, G., WHIPPLE, K.X. & HONDZO, M. (1998) Hydroplaning of Subaqueous Debris Flows. *Geological Society of America Bulletin*, **110,** 387-394.

MOSCARDELLI, L. & WOOD, L. (2008) New Classification System for Mass Transport Complexes in Offshore Trinidad. *Basin Research*, **20,** 73-98.

MOSS, G.D., CATHRO, D.L. & AUSTIN, J.A. (2004) Sequence Biostratigraphy of Prograding Clinoforms, Northern Carnarvon Basin, Western Australia: A Proxy for Variations in Oligocene to Pliocene Global Sea Level? *Palaios*, **19,** 206-226.

NARDIN, T.R., HEIN, F., GORSLINE, D.S. & EDWARDS, B. (1979) A Review of Mass Movement Processes Sediment and Acoustic Characteristics, and Contrasts in Slope and Base-of-Slope Systems Versus Canyon-Fan-Basin Floor Systems.

NEMEC, W. (1991) Aspects of Sediment Movement on Steep Delta Slopes. In: *Coarsed-Grained Deltas* (Ed. by A. Colella & D. B. Prior), **10**, 29-73. International Association of Sedimentologists.

NUGRAHA, H.D., JACKSON, C.A.L., JOHNSON, H.D., HODGSON, D.M. & REEVE, M.T. (2019) Tectonic and Oceanographic Process Interactions Archived in Late Cretaceous to Present Deep-Marine Stratigraphy on the Exmouth Plateau, Offshore Nw Australia. *Basin Research*, **31,** 405-430.

NUGRAHA, H.D., JACKSON, C.A.-L., JOHNSON, H.D. & HODGSON, D.M. (2020) Lateral Variability in Strain Along the Toewall of a Mass Transport Deposit: A Case Study from the Makassar Strait, Offshore Indonesia. *Journal of the Geological Society*, **177,** 1261-1279.

NUGRAHA, H.D., JACKSON, C.A.-L., JOHNSON, H.D., HODGSON, D.M. & CLARE, M.A. (2022) Extreme Erosion by Submarine Slides. *Geology*, **50,** 1130-1134.

NWOKO, J., KANE, I. & HUUSE, M. (2020) Megaclasts within Mass-Transport Deposits: Their Origin, Characteristics and Effect on Substrates and Succeeding Flows.

OGATA, K., MOUNTJOY, J., PINI, G.A., FESTA, A. & TINTERRI, R. (2014) Shear Zone Liquefaction in Mass Transport Deposit Emplacement: A Multi-Scale Integration of Seismic Reflection and Outcrop Data. *Marine Geology*, **356,** 50-64.

OMERU, T. & CARTWRIGHT, J.A. (2019) The Efficacy of Kinematic Indicators in a Complexly Deformed Mass Transport Deposit: Insights from the Deepwater Taranaki Basin, New Zealand. *Marine and Petroleum Geology*, **106,** 74-87.

ORTIZ-KARPF, A., HODGSON, D.M., JACKSON, C.A.-L. & MCCAFFREY, W.D. (2017) Influence of Seabed Morphology and Substrate Composition on Mass-Transport Flow Processes and Pathways: Insights from the Magdalena Fan, Offshore Colombia. *Journal of Sedimentary Research*, **87,** 189-209.

PARKER, E.J., TRAVERSO, C.M., MOORE, R., EVANS, T. & USHER, N. (2008). *Evaluation of Landslide Impact on Deepwater Submarine Pipelines*. Offshore technology conference, OTC.

PARTYKA, G., GRIDLEY, J. & LOPEZ, J. (1999) Interpretational Applications of Spectral Decomposition in Reservoir Characterization. *The Leading Edge*, **18,** 353-360.

753 POSAMENTIER, H.W. & KOLLA, V. (2003) Seismic Geomorphology and Stratigraphy of Depositional
754 Elements in Deep-Water Settings. *Journal of Sedimentary Research*, **73,** 367-388.
755 POSAMENTIER, H.W. & MARTINSEN, O.J. (2011) The Character and Genesis of Submarine Mass-Transport
756 Deposits: Insights from Outcrop and 3d Seismic Data. *Mass-transport deposits in deepwater*
757 *settings: Society for Sedimentary Geology (SEPM) Special Publication 96***,** 7-38.
758 PRÉLAT, A., PANKHANIA, S.S., JACKSON, C.A.-L. & HODGSON, D.M. (2015) Slope Gradient and Lithology as
759 Controls on the Initiation of Submarine Slope Gullies; Insights from the North Carnarvon Basin,
760 Offshore Nw Australia. *Sedimentary Geology*, **329,** 12-17.
761 PRIOR, D.B., BORNHOLD, B. & JOHNS, M. (1984) Depositional Characteristics of a Submarine Debris Flow.
762 *The Journal of Geology*, **92,** 707-727.
763 RANDOLPH, M.F. & WHITE, D.J. (2012) Interaction Forces between Pipelines and Submarine Slides—a
764 Geotechnical Viewpoint. *Ocean Engineering*, **48,** 32-37.
765 SAWYER, D.E., FLEMINGS, P.B., DUGAN, B. & GERMAINE, J.T. (2009) Retrogressive Failures Recorded in Mass
766 Transport Deposits in the Ursa Basin, Northern Gulf of Mexico. *Journal of Geophysical*
767 *Research: Solid Earth*, **114**.
768 SCARSELLI, N., MCCLAY, K. & ELDERS, C. (2013). *Submarine Slide and Slump Complexes, Exmouth Plateau,*
769 *Nw Shelf of Australia*. The Sedimentary Basins of Western Australia IV: Proceedings of the
770 Petroleum Exploration Society of Australia Symposium, Perth.
771 SOBIESIAK, M.S., KNELLER, B., ALSOP, G.I. & MILANA, J.P. (2018) Styles of Basal Interaction beneath Mass
772 Transport Deposits. *Marine and Petroleum Geology*, **98,** 629-639.
773 SOBIESIAK, M.S., BUSO, V.V., KNELLER, B., ALSOP, G.I. & MILANA, J.P. (2019) Block Generation, Deformation,
774 and Interaction of Mass-Transport Deposits with the Seafloor: An Outcrop-Based Study of the
775 Carboniferous Paganzo Basin (Cerro Bola, Nw Argentina). *Submarine Landslides: Subaqueous*
776 *Mass Transport Deposits from Outcrops to Seismic Profiles***,** 91-104.
777 STEVENTON, M.J., JACKSON, C.A.L., HODGSON, D.M. & JOHNSON, H.D. (2019) Strain Analysis of a Seismically
778 Imaged Mass-Transport Complex, Offshore Uruguay. *Basin Research*, **31,** 600-620.
779 SUN, Q., ALVES, T., LU, X., CHEN, C. & XIE, X. (2018a) True Volumes of Slope Failure Estimated from a
780 Quartenary Mass-Transport Deposit in the Northern South China Sea. *Geophysical Research*
781 *Letters*.
782 SUN, Q., ALVES, T.M., LU, X., CHEN, C. & XIE, X. (2018b) True Volumes of Slope Failure Estimated from a
783 Quaternary Mass-Transport Deposit in the Northern South China Sea. *Geophysical Research*
784 *Letters*, **45,** 2642-2651.
785 TALLING, P.J., MASSON, D.G., SUMNER, E.J. & MALGESINI, G. (2012) Subaqueous Sediment Density Flows:
786 Depositional Processes and Deposit Types. *Sedimentology*, **59,** 1937-2003.
787 TINDALE, K., NEWELL, N., KEALL, J. & SMITH, N. (1998) Structural Evolution and Charge History of the
788 Exmouth Sub-Basin, Northern Carnarvon Basin, Western Australia. In: *The Sedimentary Basins*
789 *of Western Australia 2: Proceedings of the Petroleum Exploration Society of Australia* (Ed. by
790 P. G. Purcell & R. R. Purcell), 473-490, Perth.
791 TRINCARDI, F. & ARGNANI, A. (1990) Gela Submarine Slide: A Major Basin-Wide Event in the Plio-
792 Quaternary Foredeep of Sicily. *Geo-Marine Letters*, **10,** 13.
793 VANNESTE, M., FORSBERG, C.F., GLIMSDAL, S., HARBITZ, C.B., ISSLER, D., KVALSTAD, T.J., LØVHOLT, F. & NADIM, F.
794 (2013) Submarine Landslides and Their Consequences: What Do We Know, What Can We Do?
795 In: *Landslide Science and Practice: Volume 5: Complex Environment* (Ed. by, 5-17. Springer.
796 VARNES, D.J. (1978) Slope Movement Types and Processes. *Special report*, **176,** 11-33.
797 WU, N., JACKSON, C.A.-L., HODGSON, D.M., NUGRAHA, H.D. & ZHONG, G. (2026) Interactions between Buried
798 Mass-Transport Complexes and Subsequent Slope Failures on a Passive Margin. *Geological*
799 *Society of America Bulletin*.
800 ZAKERI, A., HØEG, K. & NADIM, F. (2008) Submarine Debris Flow Impact on Pipelines—Part I: Experimental
801 Investigation. *Coastal engineering*, **55,** 1209-1218.
802 ZAKERI, A. (2009) Review of State-of-the-Art: Drag Forces on Submarine Pipelines and Piles Caused by
803 Landslide or Debris Flow Impact.

ZENG, H., HENRY, S.C. & RIOLA, J.P. (1998) Stratal Slicing, Part Ii: Real 3-D Seismic Data. *Geophysics*, **63,** 514-522.

FIGURE CAPTIONS

Fig. 1.--- A) Location of the study area. Regional seismic line (orange) across several wells (see Fig. 2). **B)** Seabed map of the Gorgon Slide, and industry well data (red dots) available for this study. The Gorgon Slide is expressed as rugose relief on the seabed. Both evacuation and most of deposition zones are imaged within the 3D seismic reflection data. **C)** Outline of the deposits of the Gorgon Slide (dark grey), where a minor area (*c.*7%) of the total slide area in the NW (dashed line) is not imaged within the 3D seismic reflection data. This minor part is delineated using 2D seismic lines (green). Five 3D seismic reflection datasets (Gorgon, Acme, Draeck, Duyfken, and Io-Jansz) were used in this study. Bathymetry and topography data are from Geoscience Australia.

Fig. 2.--- A regional seismic section across the Exmouth Plateau (see Fig. 1 for location). **A)** Uninterpreted. **B)** Interpreted. The Gorgon Slide is bound by a basal-shear surface (yellow) at the base and seabed (blue) at the top. Modified from (Nugraha, H. D. *et al.*, 2019).

Fig. 3.--- A) Thickness map of the Gorgon Slide showing lateral boundaries of the slide (i.e. NE lateral margin and pinch-out in the SW), with thickness concentration adjacent to the NE lateral margin. We divide rugged geometry of the frontal margin into eastern and western frontal margins. **B)** Seabed dip map showing two distinct sub-bodies (namely Area A and B) within the slide. The two areas are separated by a zone of longitudinal shear. The depositional zone of the slide comprises upper (UTD) and lower (LTD) translational and toe domains. **C)** A 3D perspective of seabed structure map in the LTD showing the geometry of the longitudinal shear zone.

Fig. 4.--- A) Dip-oriented seismic section across the Gorgon Slide showing the headwall scarp, evacuation and deposition zones. **B)** Strike-oriented seismic section showing the asymmetric geometry of the slide, with erosional lateral margin in the NE and pinch-out in the SW.

828 **Fig. 5.---** Seismic facies classification used in this study. **A)** Seismic facies description and
829 interpretation. **B)** Variance attributes extraction between the basal-shear surface and an iso-
830 proportional surface (50% between the basal-shear surface and the seabed). **C-E)** Seismic sections
831 showing seismic facies within the translation domain. **F)** A time-slice of variance attribute extraction
832 (see G for position) showing seismic facies in the toe domain. **G)** A seismic section showing seismic
833 facies in the toe domain. Vertical exagerration of all seismic sections is 15.

834 **Fig. 6.---** Seabed map showing kinematic indicators in the headwall domain, which include the main
835 headwall of the Gorgon Slide, grooves, crown cracks, pockmarks, and a small scarp. **A)** Uninterpreted.
836 **B)** Interpreted.

837 **Fig. 7.---** Upper translational domain of the Gorgon Slide. **A)** Basal-shear surface variance map (top)
838 and its interpretation (bottom). **B)** Internal body RMS amplitude map (extracted 50 ms above and
839 below isoproportional horizon, orange) (top) and its interpretation (bottom). **C)** Top surface dip map
840 (top) and its interpretation (bottom). **D)** Seismic sections, uninterpreted (above) and interpreted
841 (bottom), showing seismic facies across the upper translational domain. See text for discussions.

842 **Fig. 8.--- A)** Spectral decomposition map within the slide (50% between basal-shear and top surfaces)
843 showing features within upper translational domain in detail. **B)** Uninterpreted, and **C)** interpreted,
844 seismic section along megaclasts (SF-4) across Area A and B. See text for discussion.

845 **Fig. 9.---** Lower translational domain of the Gorgon Slide. **A)** Basal-shear surface variance map (top)
846 and its interpretation (bottom). **B)** Internal body RMS amplitude map (extracted 50 ms above and
847 below isoproportional horizon, orange) (top) and its interpretation (bottom). **C)** Top surface dip map
848 (top) and its interpretation (bottom). **D)** Seismic sections, uninterpreted (above) and interpreted
849 (bottom), showing seismic facies across the upper translational domain. See text for discussion.

850 **Fig. 10.---** Dimensions and orientation of the megaclasts in the upper and translation domains. **A)**
851 Megaclasts in the upper translational domain are generally thinner with longer long-axes, as

compared to the ones in the lower translational domain that are thicker with shorter long-axes. **B)** Megaclasts in the upper translational domain are generally oriented perpendicular, and the ones in the lower translational domain are oblique to sub-parallel, to the transport direction.

Fig. 11.--- Toe domain of the Gorgon Slide. **A)** Basal-shear surface variance map (top) and its interpretation (bottom). **B)** Internal body RMS amplitude map (time-slice at the orange horizon in D) (top) and its interpretation (bottom). **C)** Top surface dip map (top) and its interpretation (bottom). **D)** Seismic sections, uninterpreted (above) and interpreted (bottom), showing seismic facies across the toe domain. See text for discussion.

Fig. 12.--- Schematic diagram of Gorgon Slide depicting three stages of emplacement processes. **A)** A failure event occurred. **B)** The slide split into two flow cells, Cell A and B, due to a cluster of megaclasts derived from the headwall and/or slope strata that acted as a flow obstacle. **C)** Cell A ceased, and its frontal margin is expressed on the seabed, while Cell B flowed beyond the limit of the dataset. See text for discussion.

865 Fig. 1

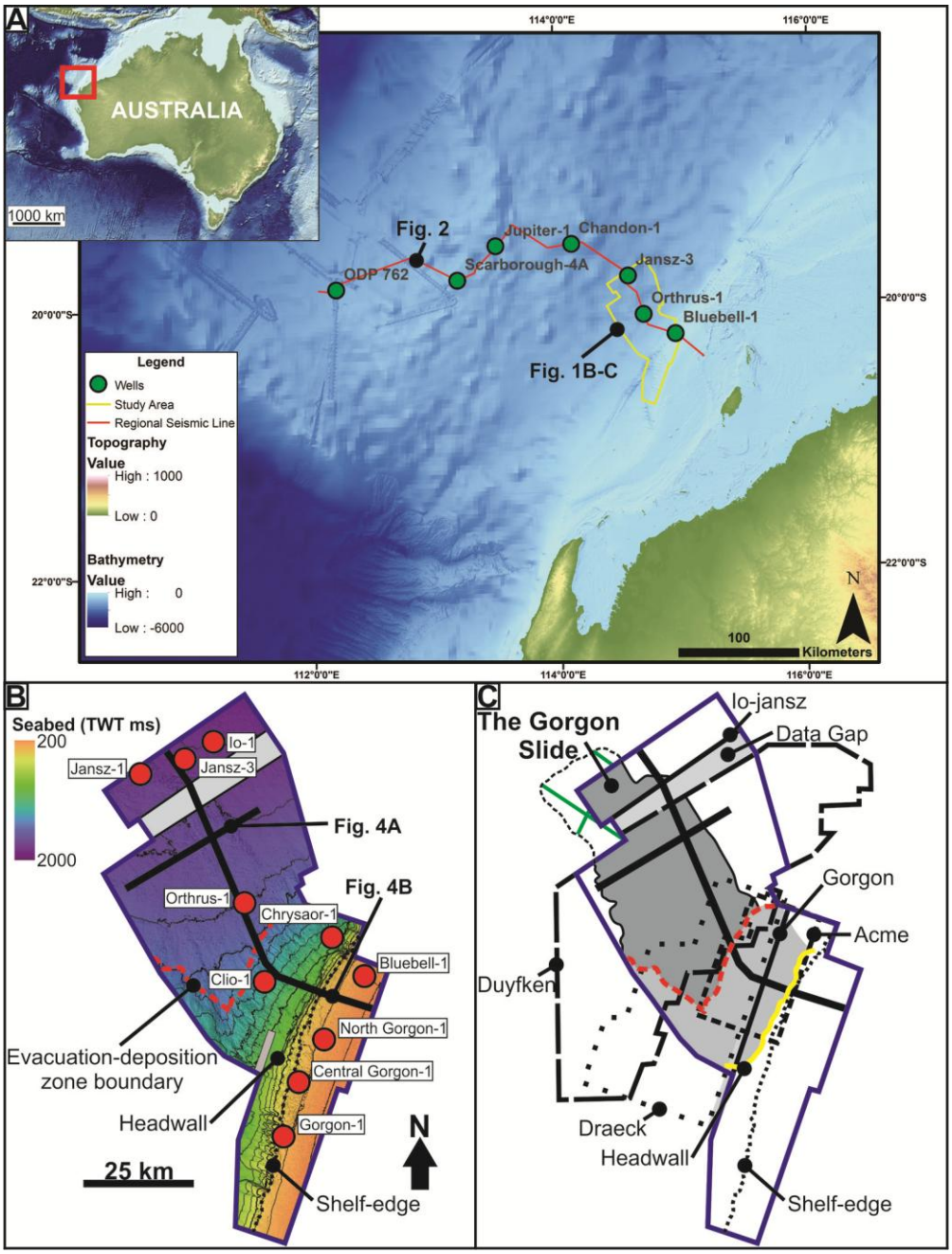
A
AUSTRALIA
1000 km
114°0'0"E
116°0'0"E
20°0'0"S
22°0'0"S
112°0'0"E
Fig. 2
Jupiter-1
Chandon-1
Scarborough-4A
Jansz-3
ODP 762
Orthrus-1
Bluebell-1
Fig. 1B-C
Legend
Wells
Study Area
Regional Seismic Line
Topography
Value
High : 1000
Low : 0
Bathymetry
Value
High : 0
Low : -6000
N
100
Kilometers
B
Seabed (TWT ms)
200
2000
Io-1
Jansz-1
Jansz-3
Fig. 4A
Fig. 4B
Orthrus-1
Chrysaor-1
Bluebell-1
Clio-1
North Gorgon-1
Central Gorgon-1
Evacuation-deposition zone boundary
Headwall
Gorgon-1
N
25 km
Shelf-edge
C
The Gorgon Slide
Io-jansz
Data Gap
Gorgon
Acme
Duyfken
Draeck
Headwall
Shelf-edge

866

867 Fig. 2

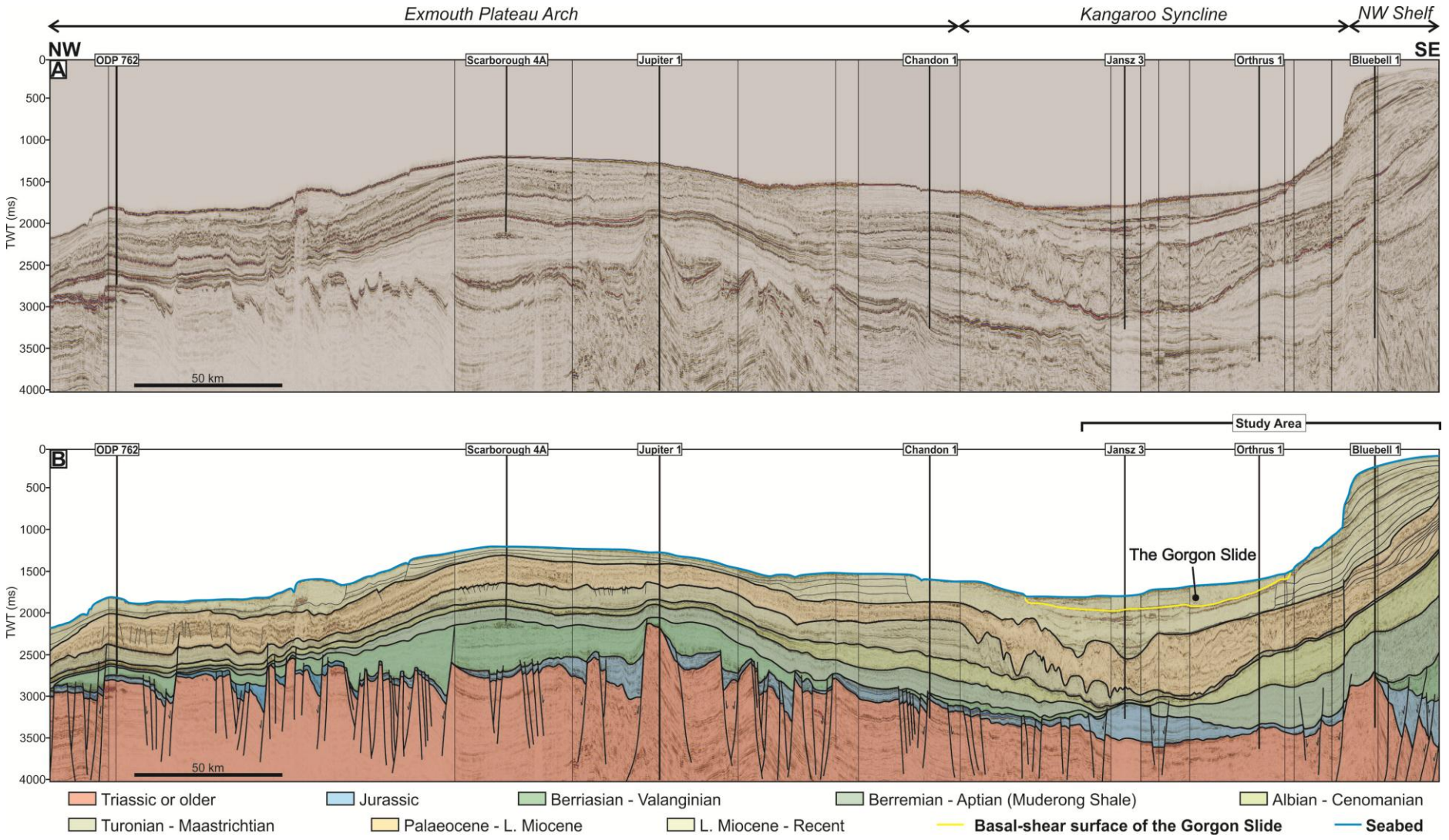
Exmouth Plateau Arch
Kangaroo Syncline
NW Shelf
NW
SE
A
B
ODP 762
Scarborough 4A
Jupiter 1
Chandon 1
Jansz 3
Orthrus 1
Bluebell 1
TWT (ms)
0
500
1000
1500
2000
2500
3000
3500
4000
50 km
Study Area
The Gorgon Slide
Triassic or older
Jurassic
Berriasian - Valanginian
Berremian - Aptian (Muderong Shale)
Albian - Cenomanian
Turonian - Maastrichtian
Palaeocene - L. Miocene
L. Miocene - Recent
Basal-shear surface of the Gorgon Slide
Seabed

868

869 Fig. 3

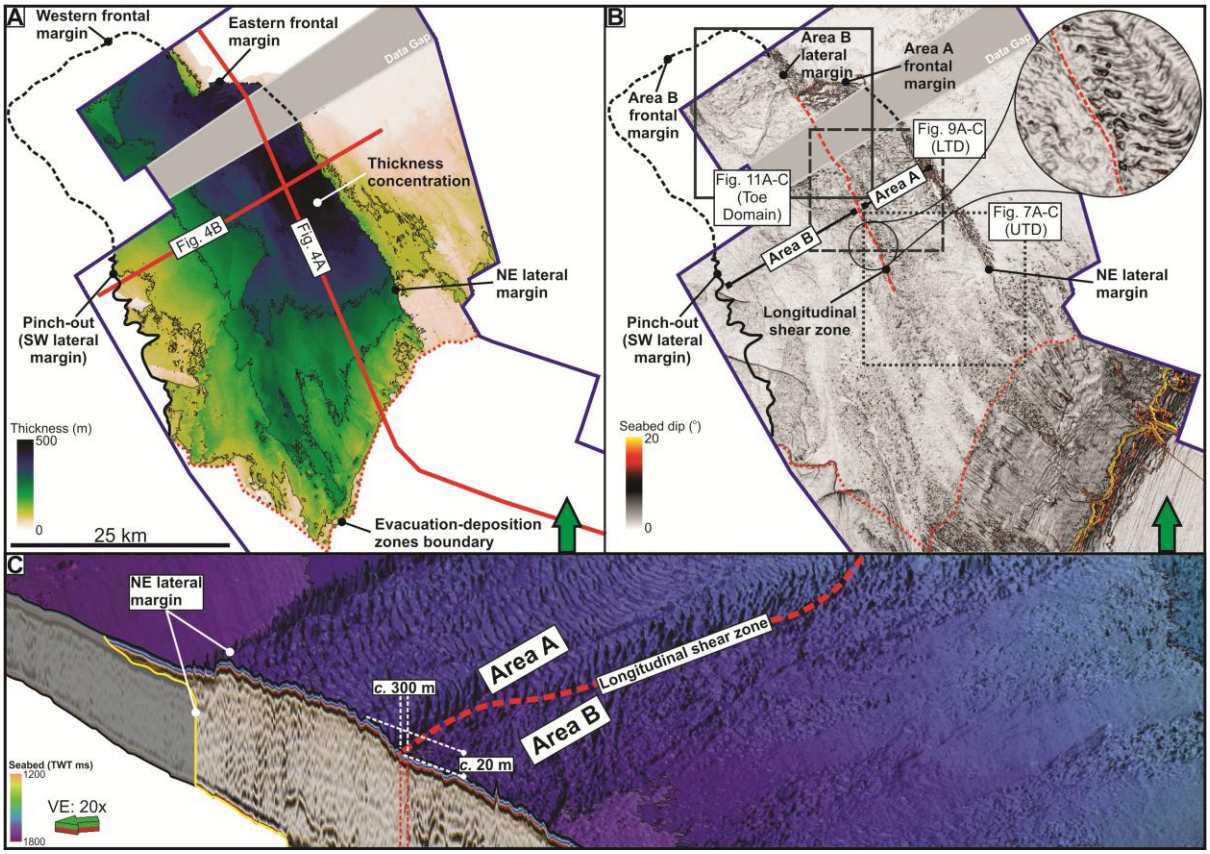

870

871

872 Fig. 4

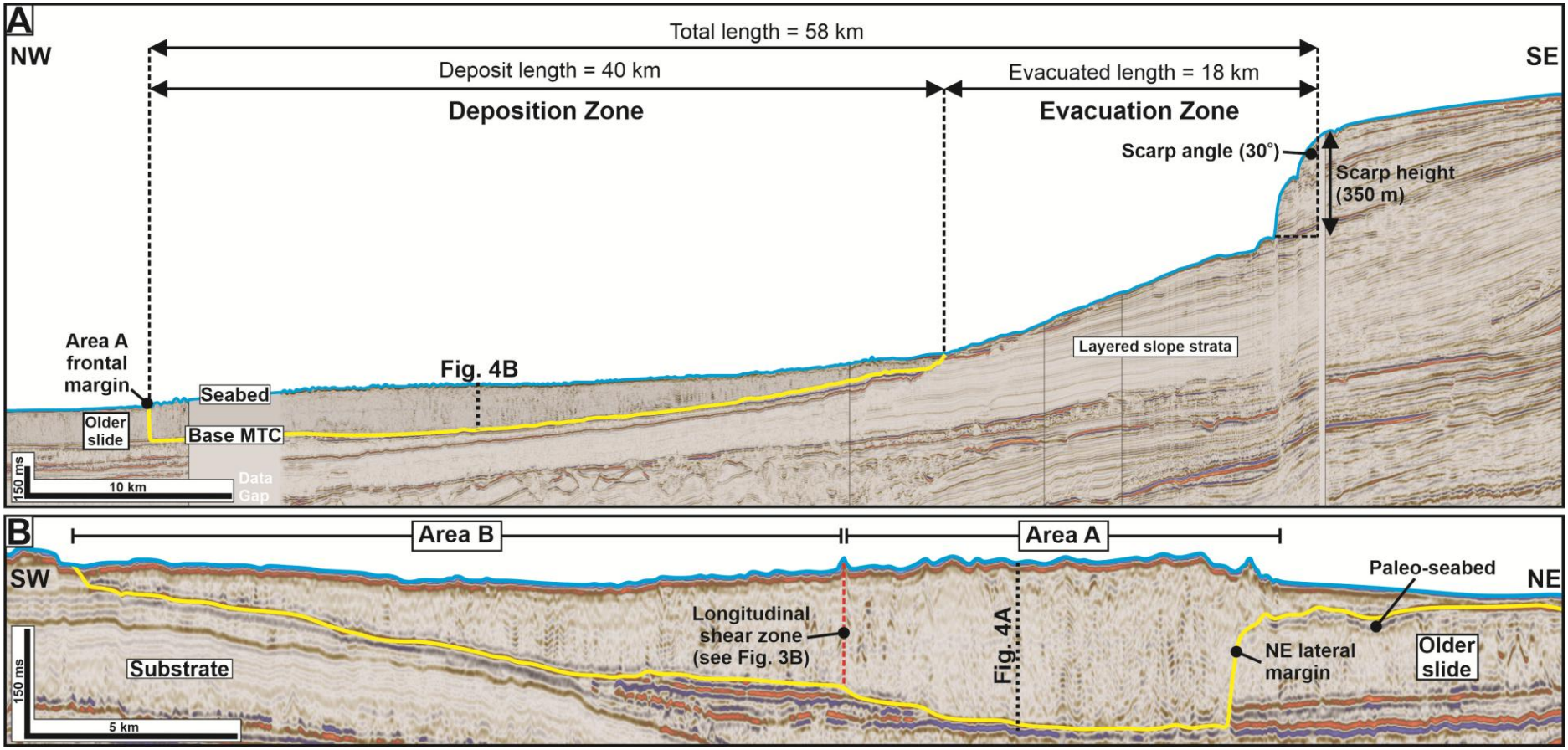
A
NW
SE
Total length = 58 km
Deposit length = 40 km
Deposition Zone
Evacuated length = 18 km
Evacuation Zone
Scarp angle (30°)
Scarp height (350 m)
Area A frontal margin
Seabed
Older slide
Base MTC
Fig. 4B
Layered slope strata
150 ms
10 km
Data Gap
B
Area B
Area A
SW
NE
Paleo-seabed
Longitudinal shear zone (see Fig. 3B)
Fig. 4A
NE lateral margin
Older slide
Substrate
150 ms
5 km

873

874 Fig. 5

A Facies	Description	Interpretation
SF-1	Chaotic and transparent both in cross-section and map-view (Fig. 5B-C).	Debrites containing disaggregated materials (cf. Posamentier and Kolla 2003).
SF-2	Low-to-medium amplitude, discontinuous folded reflections that occasionally form sinuous lineations in map-view (Fig. 5B, D-E).	Debrites containing partially disaggregated materials (cf. Ortiz-Karpf et al. 2017).
SF-3	High amplitude, discontinuous folded reflections that are separated by imbricate thrusts (Fig. 5F-G).	Fold and thrust systems formed by compressional deformation within MTCs, flow direction is generally perpendicular to the strike of the thrusts (Bull et al. 2009).
SF-4	Isolated packages of coherent, sub-parallel reflections within a matrix composed of SF-1 or 2 (Fig. 5B-C, E). In most cases, the reflections are disrupted, e.g. faulted and folded.	Megaclasts transported within debritic matrix (cf. Bull et al. 2009; Jackson 2011; Hodgson et al. 2018).
SF-5	Medium-to-high amplitude, continuous, sub-parallel, downslope-dipping reflections beneath the shelf and within the evacuation zone (Fig. 4A).	Non-MTC deposits, i.e. carbonate progradation and layered slope deposits that were the source of, and eroded by, the Gorgon Slide (Hengesh et al. 2013; Nugraha et al. 2019b).

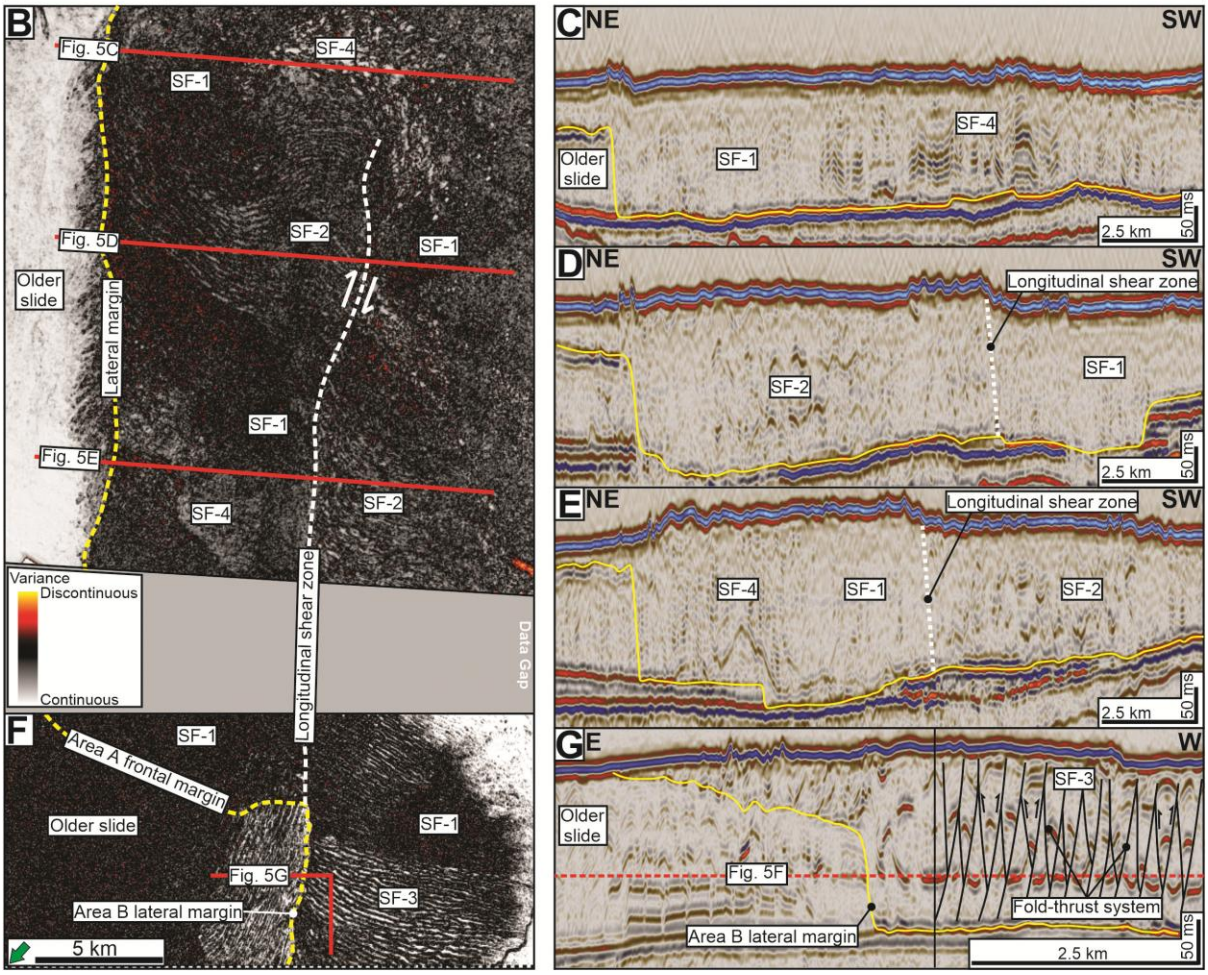

875

876 Fig. 6

877

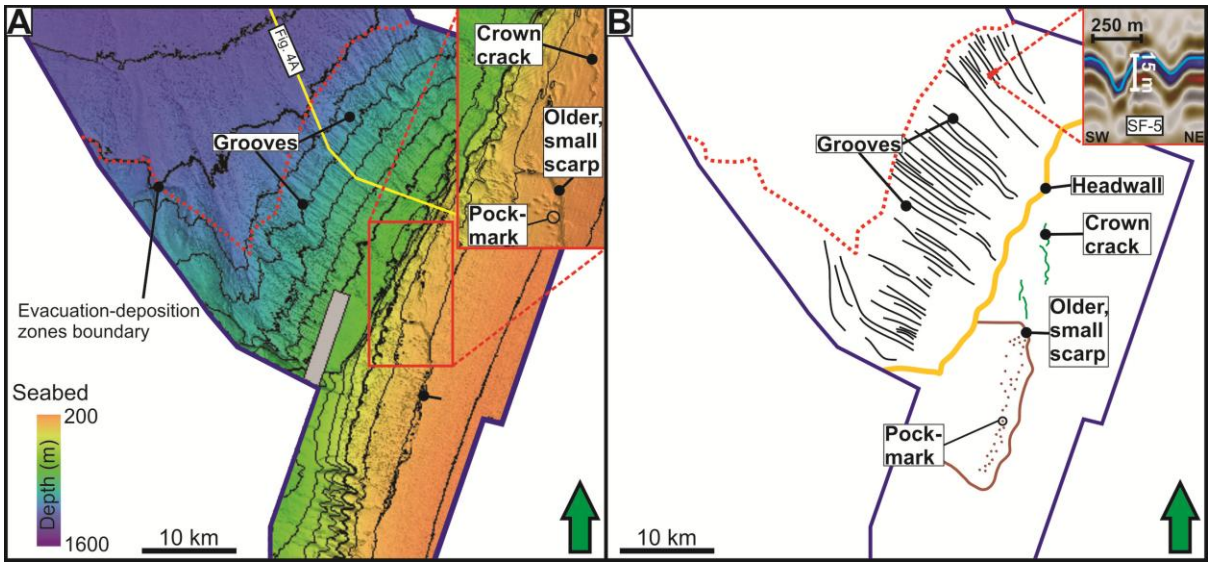
A
Fig. 4A
Crown crack
Grooves
Older, small scarp
Pock-mark
Evacuation-deposition zones boundary
Seabed
200
Depth (m)
1600
10 km
B
250 m
SF-5
SW
NE
Grooves
Headwall
Crown crack
Older, small scarp
Pock-mark
10 km

878 Fig. 7

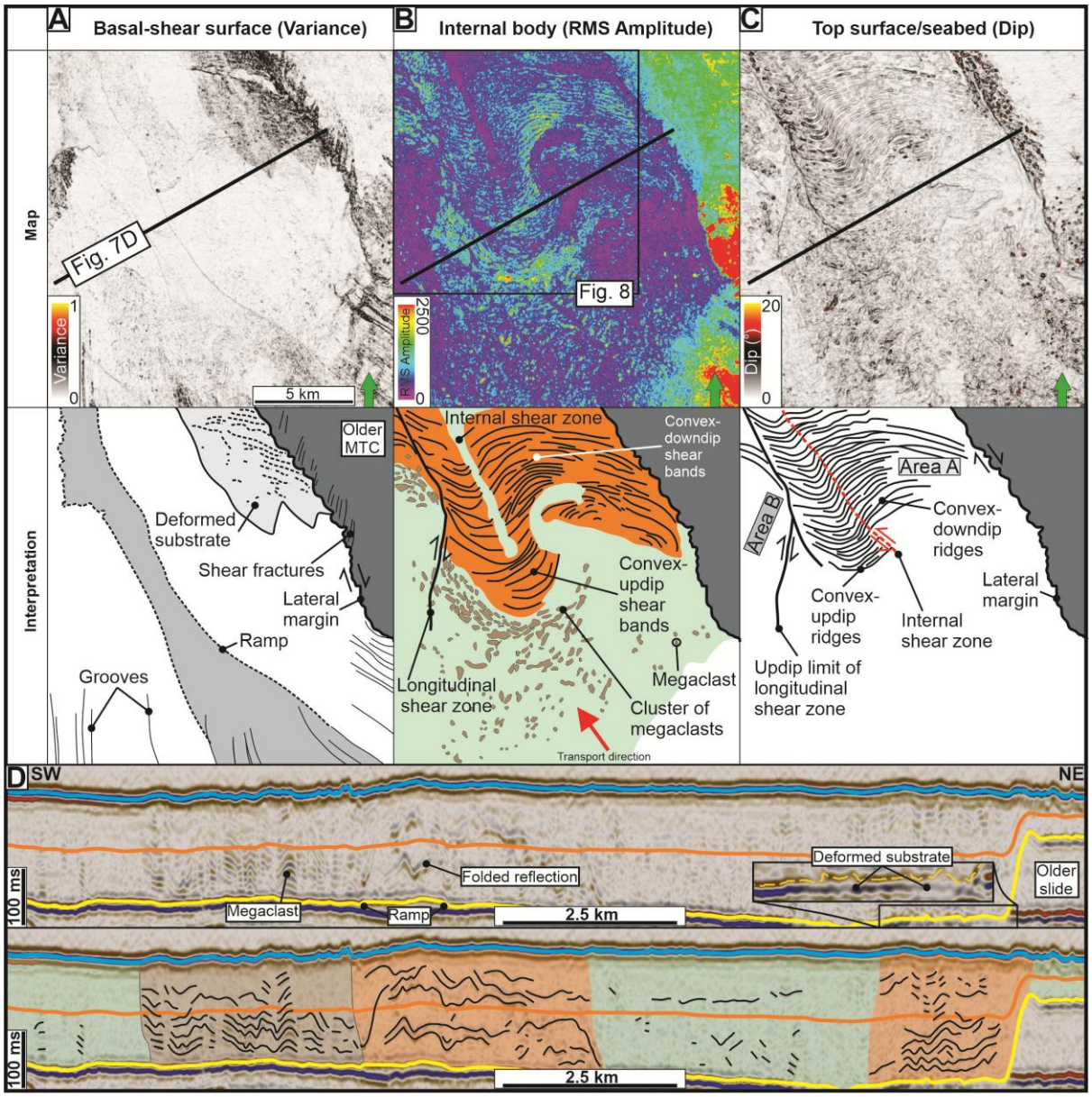
A
Basal-shear surface (Variance)
B
Internal body (RMS Amplitude)
C
Top surface/seabed (Dip)
Map
Fig. 7D
Fig. 8
Variance
1
0
RMS Amplitude
2500
0
Dip (°)
20
0
5 km
Interpretation
Older MTC
Deformed substrate
Shear fractures
Lateral margin
Ramp
Grooves
Internal shear zone
Convex-downdip shear bands
Convex-updip shear bands
Megaclast
Longitudinal shear zone
Cluster of megaclasts
Transport direction
Area A
Area B
Convex-downdip ridges
Convex-updip ridges
Internal shear zone
Lateral margin
Updip limit of longitudinal shear zone
D
SW
NE
100 ms
Megaclast
Ramp
Folded reflection
2.5 km
Deformed substrate
Older slide
100 ms
2.5 km
Seismic facies within the Gorgon Slide
SF-1
SF-2
SF-3
SF-4

879

880 Fig. 8

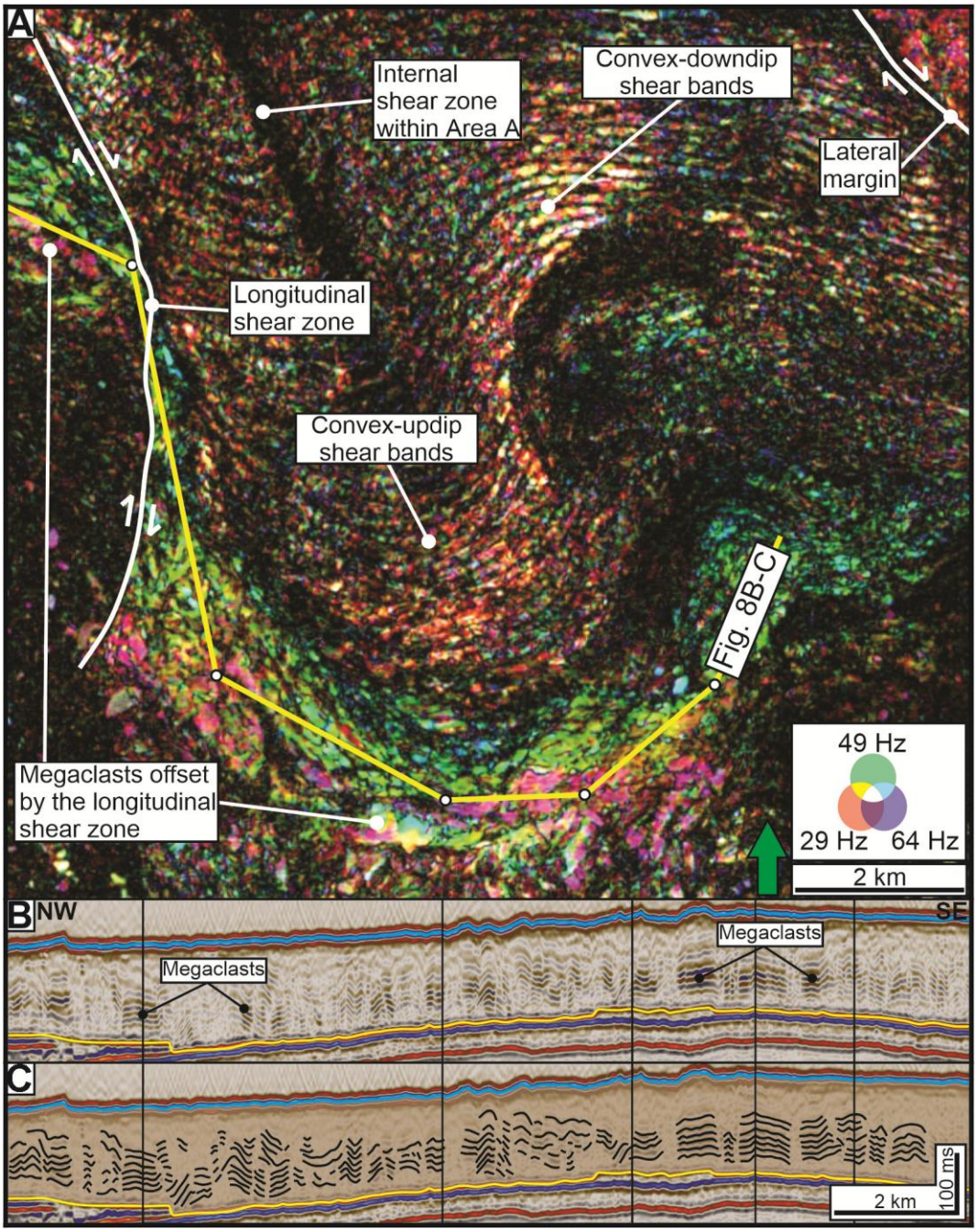
A
Internal shear zone within Area A
Convex-downdip shear bands
Lateral margin
Longitudinal shear zone
Convex-updip shear bands
Fig. 8B-C
Megaclasts offset by the longitudinal shear zone
49 Hz
29 Hz
64 Hz
2 km
B
NW
SE
Megaclasts
Megaclasts
C
2 km
100 ms

881

882 Fig. 9

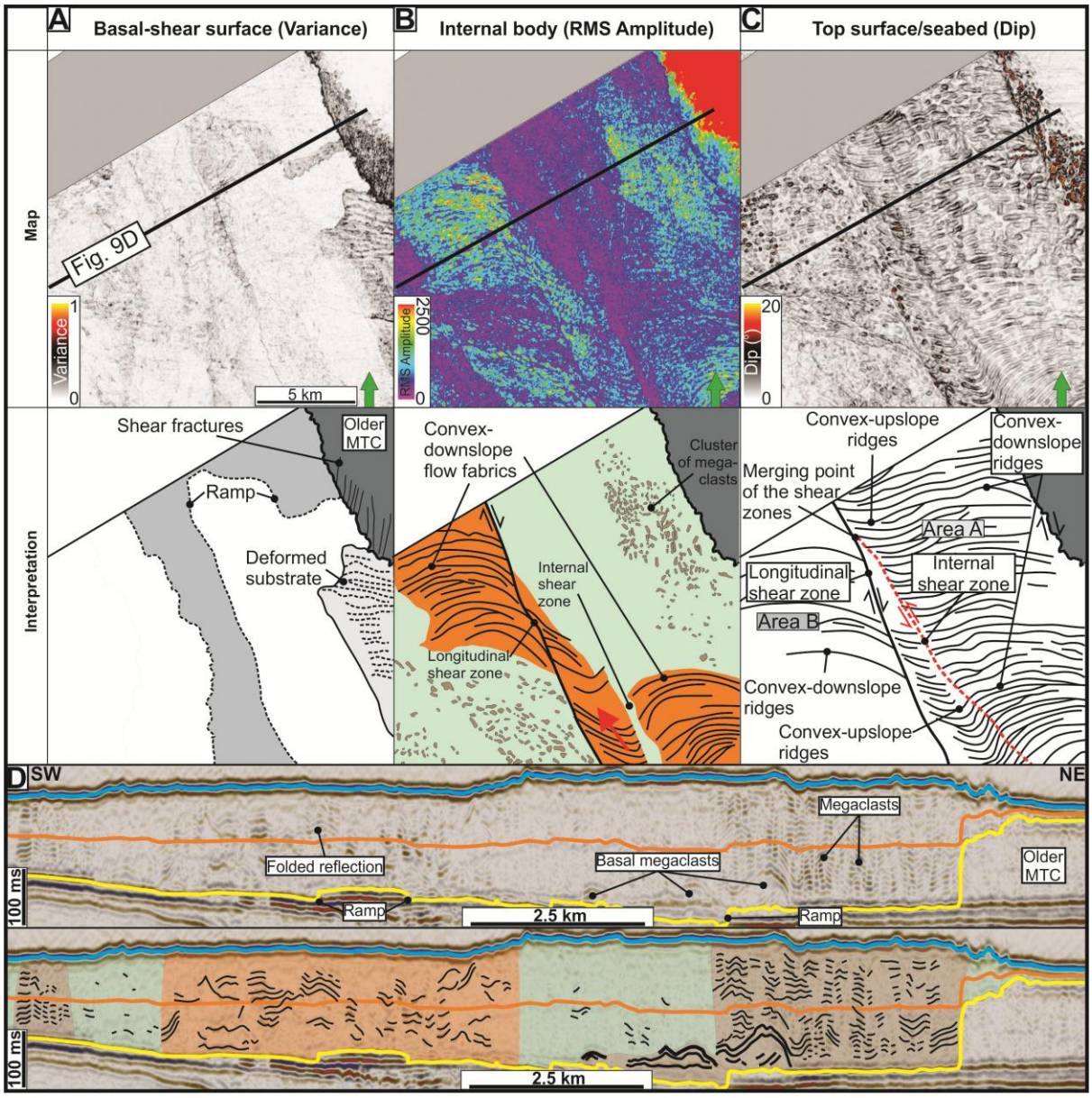
A
Basal-shear surface (Variance)
B
Internal body (RMS Amplitude)
C
Top surface/seabed (Dip)
Map
Fig. 9D
Variance
1
0
5 km
RMS Amplitude
2500
0
Dip (°)
20
0
Interpretation
Shear fractures
Older MTC
Ramp
Deformed substrate
Convex-downslope flow fabrics
Cluster of mega-clasts
Internal shear zone
Longitudinal shear zone
Convex-upslope ridges
Convex-downslope ridges
Merging point of the shear zones
Area A
Area B
Longitudinal shear zone
Internal shear zone
Convex-downslope ridges
Convex-upslope ridges
D
SW
NE
Megaclasts
Folded reflection
Basal megaclasts
Older MTC
Ramp
2.5 km
Ramp
100 ms
100 ms
2.5 km
Seismic facies within the Gorgon Slide
SF-1
SF-2
SF-3
SF-4

883

884 Fig. 10

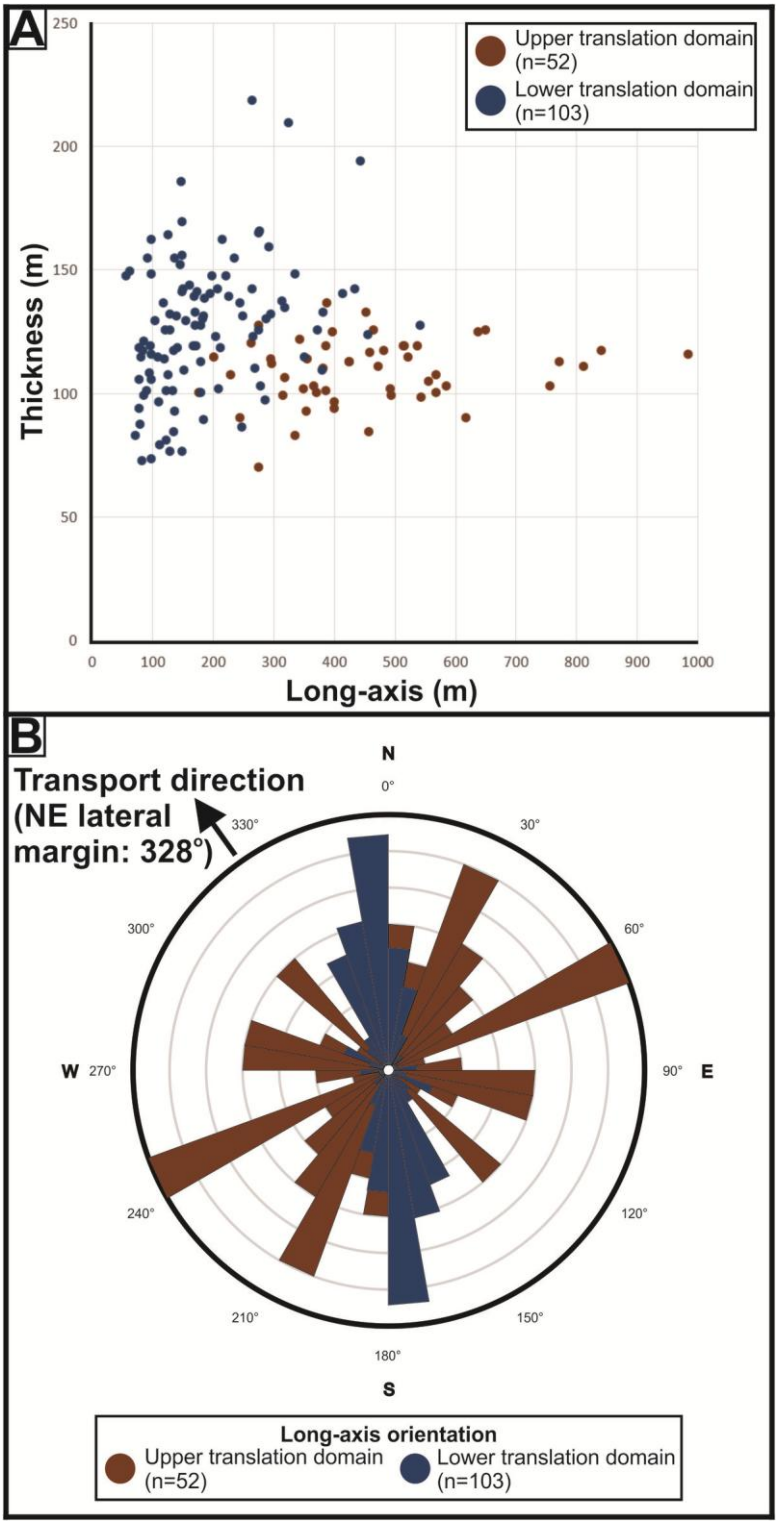

885

886 Fig. 11

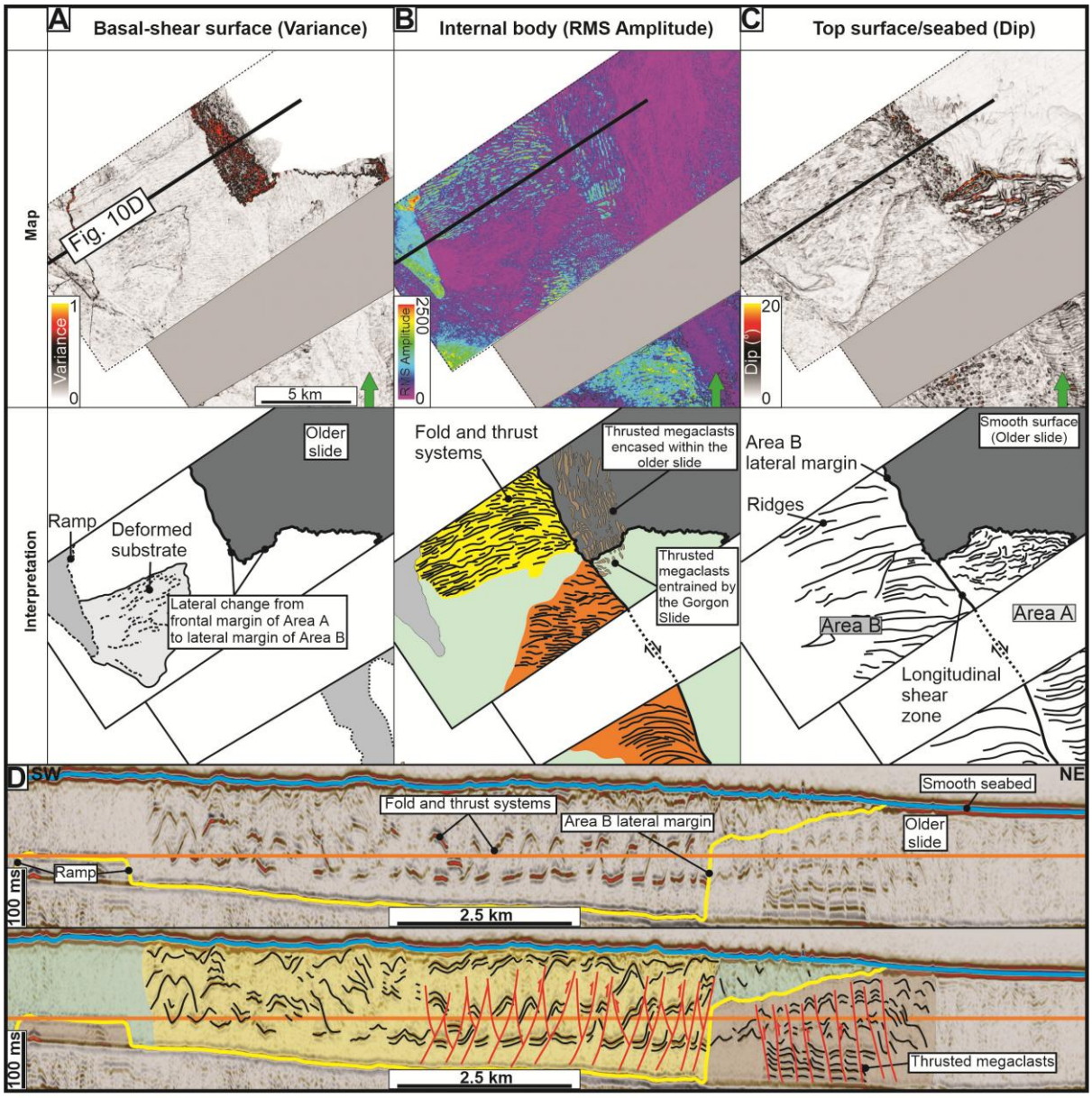

887

888 Fig. 12

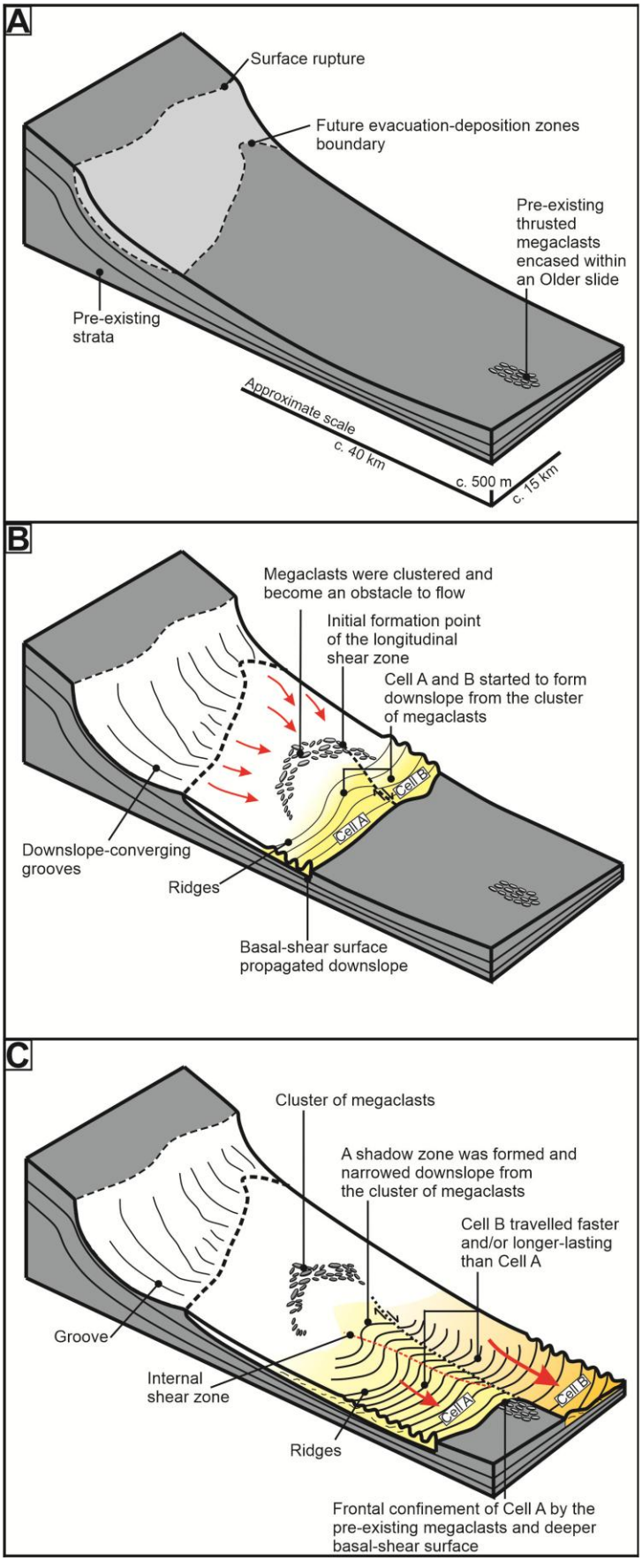

889